Correspondence to:
D. L. Harry,
Dennis.Harry@colostate.edu

Evolution of the Southwest Australian Rifted Continental Margin During Breakup of East Gondwana: Results From International Ocean Discovery Program Expedition 369

D. L. Harry[1], M. L. G. Tejada[2], E. Y. Lee[3], E. Wolfgring[4], C. C. Wainman[5], H.-J. Brumsack[6], B. Schnetger[6], J.-I. Kimura[2], L. Riquier[7], I. Borissova[8], R. W. Hobbs[9], T. Jiang[10], Y-X. Li[11], A. Maritati[12], M. Martinez[13], C. Richter[14], G. Tagliaro[15], and L. T. White[16]

[1]Department of Geosciences, Colorado State University, Fort Collins, CO, USA, [2]Institute for Marine Geodynamics, Japan Agency for Marine-Earth Science and Technology, Yokosuka-shi, Kanagawa, Japan, [3]Faculty of Earth Systems and Environmental Sciences, Chonnam National University, Gwangju, Republic of Korea, [4]Department of Geodynamics and Sedimentology, University of Vienna, Vienna, Austria, [5]Australian School of Petroleum and Energy Resources, University of Adelaide, Adelaide, Australia, [6]Institut für Chemie und Biologie Des Meeres (ICBM), Carl von Ossietzky Universität Oldenburg, Oldenburg, Germany, [7]Institut des Sciences de la Terre de Paris (ISTeP), Sorbonne University, Paris, France, [8]Petroleum and Marine Division, Geoscience Australia, Canberra, Australia, [9]Department of Earth Sciences, University of Durham, Durham, UK, [10]Department of Marine Science and Engineering, China University of Geosciences, Wuhan, P.R. China, [11]School of Earth Sciences and Engineering, Nanjing University, Nanjing, P.R. China, [12]Institute of Marine and Antarctic Studies (IMAS), University of Tasmania, Hobart, Australia, [13]Univ Rennes, CNRS, Géosciences Rennes, Rennes, France, [14]School of Geosciences, University of Louisiana at Lafayette, Lafayette, LA, USA, [15]Department Institute for Geophysics, University of Texas at Austin, Austin, TX, USA, [16]GeoQuEST Research Centre, School of Earth, Atmospheric and LifeSciences, University of Wollongong, Wollongong, NSW, Australia

Abstract International Ocean Discovery Program Expedition 369 drilled four sites on the southwestern Australian continental margin, in the deep water Mentelle Basin (MB) and on the neighboring Naturaliste Plateau (NP). The drillsites are located on continental crust that continued rifting after seafloor spreading began further north on the Perth Abyssal Plain (PAP) between magnetochrons M11r and M11n (133–132 Ma), ending when spreading began west of the NP between chrons M5n and M3n (126–124 Ma). Drilling recovered the first in situ samples of basalt flows overlying the breakup unconformity on the NP, establishing a magnetostratigraphically constrained eruption age of >131–133 Ma, and confirming a minimal late Valanginian age for the breakup unconformity (coeval with the onset of PAP seafloor spreading). Petrogenetic modeling indicates the basalts were generated by 25% melting at 1.5 GPa and a potential temperature of 1380°C–1410°C, consistent with proximity of the Kerguelen plume during breakup. Benthic foraminiferal fossils indicate that the NP remained at upper bathyal or shallower depths during the last 6 Myr of rifting and for 3–5 Myr after breakup between India and Australia. The limited subsidence is attributed to heat from the nearby Kerguelen plume and PAP spreading ridge. The margin subsided to middle bathyal depths by Albian time and to lower bathyal (NP) or greater (MB) depths by late Paleogene time. Periods of rapid sedimentation accompanied a westward jump of the PAP spreading ridge (108 Ma), rifting on the southern margin (100–84 Ma), and opening of the southern seaway between Australia and Antarctica (60–47 Ma).

Plain Language Summary The southwestern Australian margin formed during the breakup of the supercontinent Gondwana during the Late Jurassic and Early Cretaceous Periods. International Ocean Discovery Program Expedition 369 drilled four sites on the southwestern Australian rifted continental margin in order to better understand the subsidence and magmatic behavior of the margin during the final stages of rifting. Drilling shows that a widespread unconformity imaged in seismic data on the margin correlates with the onset of seafloor spreading on the Perth Abyssal Plain at 132–133 Ma. This was followed by eruption of basalts on the Naturaliste Plateau, which were generated from melting of the underlying mantle that was enhanced by the nearby Kerguelen mantle plume. Proximity of the plume kept the margin at shallow depths during rifting and for about 3–5 Myr after final separation of India and Australia at 126 Ma. The margin subsided to > 1,000 m depths between about 121 Ma and the present,

with intervening periods of relatively rapid sedimentation associated with adjustments to the spreading ridge configuration in the Indian Ocean at 108 Ma, and rifting events between southwestern Australia and Antarctica at 100–84 Ma and 60–47 Ma.
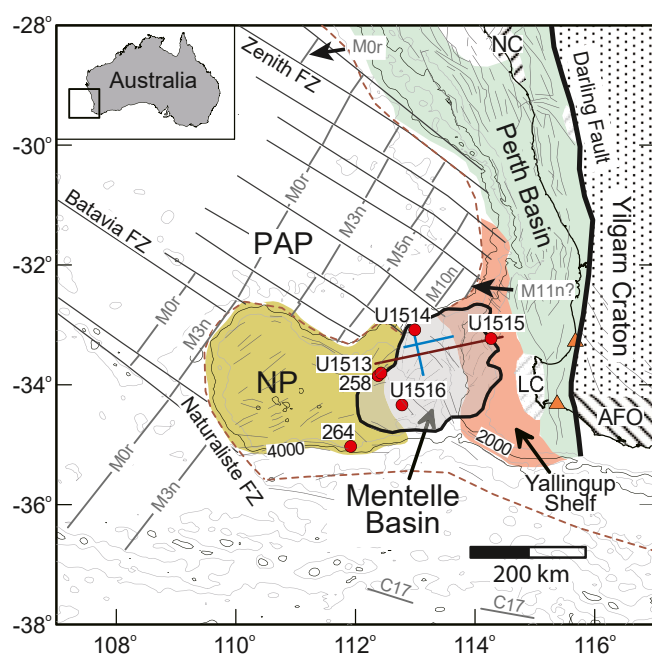
1. Introduction

In this study, we present new constraints on the late syn- and postrift evolution of the southwestern Australian continental margin from boreholes drilled during International Ocean Discovery Program (IODP) Expedition 369. The western Australian margin formed as a result of Late Jurassic through Early Cretaceous rifting as Greater India separated from Australia during the breakup of East Gondwana (the discussion here follows Gibbons et al., 2012, with ages modified to fit recent revisions to the geomagnetic time scale as discussed in Section 2.1). Rift basins formed beneath the continental shelf along most of the western Australian margin during this time, reactivating Permian rift structures in many areas (Hall et al., 2013; Yeates et al., 1987). On the southwestern part of the margin, extension occurred in the Perth Basin beneath the continental shelf and in the deep water Mentelle Basin and on the Naturaliste Plateau further offshore (Figure 1). Breakup was diachronous, with seafloor spreading beginning on the Perth Abyssal Plain no later than chron M10N (131 Ma) and between M11r and M11n (133–132 Ma) on the central part of the margin. Seafloor spreading did not begin until between chrons M5n and M3n (126–124 Ma) on the southwestern part of the margin, west of the Naturaliste Plateau. The culmination of rifting between Greater India and Australia is thus marked by two breakup events. The first, which we refer to as the Perth Abyssal Plain breakup event, occurred when seafloor spreading was established on the Perth Abyssal Plain and produced a widely recognizable breakup unconformity in the Perth Basin. The second, which we refer to as the Naturaliste Plateau breakup event, occurred when seafloor spreading was established west of the Naturaliste Plateau. During the 6–9 Myr period between the two breakup events, the spreading ridge in the Perth Abyssal Plain migrated westward along the northern margins of the Mentelle Basin and Naturaliste Plateau. The Perth Abyssal Plain breakup event was followed soon after by eruption of basalt flows, which lie on top of the breakup unconformity on the Naturaliste Plateau, in the western Mentelle Basin, and in the southern Perth Basin (Direen et al., 2017; Frey et al., 1996; Olierook et al., 2016). The culminating tectonic event on the margin was the Cretaceous through Eocene rifting episode that led to opening of the Southern Ocean between Australia and Antarctica. This rifting event began around 100 Ma on the southern margin of western Australia, leading to slow spreading by about 84 Ma that propagated eastward until separation of the South Tasman Rise from Antarctica at about 45 Ma (Cande & Mutter, 1982; Lawver et al., 1992; Mutter et al., 1985; Sayers et al., 2001; Tikku & Cande, 1999; Tikku & Direen, 2008; Veevers, 1986, 2006; L. T. White et al., 2013; Williams et al., 2013). IODP Expedition 369 obtained the first in situ record of the volcanic sequence on the Naturaliste Plateau and a complete record of the late syn- and postrift strata on the southwestern Australian margin in order to understand the magmatic and subsidence histories of the margin and their relations to the tectonic events described above (Hobbs et al., 2019; Huber et al., 2018).

Figure 1. Naturaliste Plateau (NP), Perth Abyssal Plain (PAP), Mentelle Basin, and Perth Basin. Fracture zones and seafloor spreading isochrons (gray lines) from Borissova, (2002) and Gibbons et al. (2012), with isochron names modified to use more recent notation (Table 1). The Mentelle Basin is subdivided into an eastern part that overlies the central and western Yallingup Shelf, and a western part that includes the deep water basin and a portion overlying the eastern edge of the Naturaliste Plateau (Borissova et al., 2010). Ocean-continent transition (brown dashed line) after (Hall et al., 2013; Williams et al., 2011). Darling Fault (heavy black line) and other faults (thin gray lines) after (Borissova et al., 2010; Hall et al., 2013). Labeled red circles—Deep Sea Drilling Project (2xx) and International Ocean Discovery Program (U15xx) drilling sites; triangles—Bunbury Basalt outcrops; AFO, Albany-Fraser Orogen; LC, Leeuwin Complex; NC, Northampton Complex. Thin light gray lines show bathymetry (contour interval = 1,000 m). Thick red line indicates location of seismic profile S310-05 shown in Figure 3. Blue lines show locations of seismic profiles S310-03 (trending WSW) and S310-17 (trending NNW) shown in Figure 9.

2. Geological Background

2.1. Plate Motions and Seafloor Spreading

The timing of continental breakup in the northeastern Indian Ocean and on the southwestern Australian margin is constrained primari-

ly from seafloor spreading magnetic anomalies (e.g., Ali & Aitchison, 2014; Direen et al., 2017; Gaina et al., 2007; Gibbons et al., 2012, 2013; Hall et al., 2013; Watson et al., 2016; L. T. White et al., 2013; Whittaker et al., 2016; Williams et al., 2013 and earlier references found in those papers). In this study, we use the magnetic anomaly identifications described in the plate reconstructions of Gibbons et al. (2012) and Williams et al. (2013). The ages assigned to the Cenozoic magnetic chrons are from the time scale of Ogg et al. (2016). The Late Cretaceous chron ages are from Malinverno et al. (2012), with the ages of chrons M0r through M11r revised here to match the Valanginian to Barremian stage ages indicated by recent radio-astrochronological data integrated with bio- and chemostratigraphy (Aguirre-Urreta et al., 2019; Bodin et al., 2006; Frau et al., 2018; Martinez et al., 2013; Olierook, Jourdan et al., 2019) (Tables 1 and 2). From these works, the Hauterivian Stage started at 131.3 ± 0.2 Ma, the Barremian Stage at 126.1 ± 0.2 Ma, and the Aptian Stage at 121.5 ± 0.2 Ma. The revised stage and chron ages imply ages for the Early Cretaceous events described below that are 3–5 Myr younger than in the plate reconstructions of Gibbons et al. (2012, 2013).

Opening of the Indian Ocean was preceded by a Permian extensional episode that created a rift system with branches between Australia and Antarctica and on either side of India (Harrowfield et al., 2005; Maritati et al., 2020; Veevers, 2006; Yeates et al., 1987) (Figure 2a). This was followed by a period of tectonic quiescence and regional subsidence extending into Middle Jurassic time, punctuated with minor extensional events during the Triassic and Early Jurassic Periods (Norvick, 2004; Plumb, 1979). Rifting was renewed during the Middle Jurassic Period as East and West Gondwana began to separate (Besse & Courtillot, 1988; Lawver et al., 1992; Norton & Sclater, 1979; C. M. Powell et al., 1988; Royer & Sandwell, 1989). This was accompanied by counterclockwise rotation of India away from Australia/Antarctica, resulting in northwest oriented extension on the western Australian margin and minor extension between Australia and Antarctica beginning about 165 Ma (Ball et al., 2013; Direen et al., 2008, 2011; Gibbons et al., 2013; Lawver et al., 1992; C. M. Powell et al., 1988) (Figure 2b). At this time, the Naturaliste Plateau was located at the juncture of the Indian Plate and the future boundary between the Australian and Antarctic plates. Two smaller continental blocks, Batavia and Gulden Draak Knolls, lay respectively to the north and southwest of the Naturaliste Plateau (Gibbons et al., 2013; Whittaker et al., 2016; Williams et al., 2013). Seafloor spreading between Greater India and Australia began on the Cuvier Abyssal Plain bordering the northwestern Australian margin, where it was underway by anomaly M11n to M10N time (132–131 Ma) (Fullerton et al., 1989; Gibbons et al., 2012; Heine & Müller, 2005; Markl, 1978; Robb et al., 2005). This was contemporaneous with or followed soon after by seafloor spreading on the Perth Abyssal Plain bordering the central western Australian margin (the Perth Abyssal Plain breakup event), which was also underway by anomaly M11n to M10N time (Gibbons et al., 2012; Markl, 1974, 1978; C. M. Powell et al., 1988; Williams et al., 2013) (Figure 2c). Seafloor spreading was not established west of the Naturaliste Plateau (the Naturaliste Plateau breakup event) until anomaly M5n to M3n time (126–124 Ma) (Gibbons et al., 2012; Müller et al., 2000) (Figure 2d).

The difference in ages of breakup west of the Naturaliste Plateau and on the Perth Abyssal Plain indicates that extension continued on the Naturaliste Plateau/Mentelle Basin portion of the southwestern Australian margin for ca. 6–9 Myr after seafloor spreading had begun further north. The spreading ridge on the Perth Abyssal Plain migrated westward along the northern Mentelle Basin and Naturaliste Plateau margins during this period, followed by a westward jump at anomaly M0r time (121.8 Ma) (Gibbons et al., 2012). Gulden Draak and Batavia Knolls remained attached to the Indian plate until about 108 Ma, when the ridge again jumped westward and transferred these continental fragments to the Australian plate (Whittaker et al., 2016; Williams et al., 2013) (Figure 2e).

A change in plate motions occurred at about 100 Ma as India began to move northward (Gibbons et al., 2012, 2013; Mathews et al., 2012; Whittaker et al., 2013, 2016) (Figure 2f). This was accompanied by reorientation of the Indian Ocean spreading system and the onset of rifting between Australia and Antarctica. A period of either slow seafloor spreading (Ball et al., 2013; Cande & Mutter, 1982; Müller et al., 2000; Mutter et al., 1985) and/or mantle exhumation (Direen et al., 2011; L. T. White et al., 2013) began diachronously between about 84 and 47 Ma as spreading propagated eastward along the southern margin (Figures 2g and 2h). Steady state seafloor spreading and generation of new basaltic oceanic crust was underway between Australia and Antarctica by chron C21 to C19 time (47–42 Ma) (Direen et al., 2011; Gibbons et al., 2012; Mutter et al., 1985; L. T. White et al., 2013; Williams et al., 2013).

Table 1
Cretaceous Geomagnetic Time Scales and Ages of Seafloor Spreading Anomalies

		Geologic time scales								Key spreading anomalies			
		Gee and Kent (2007)		Ogg et al. (2016)		Malinverno et al. (2012)			This study[a]		Gibbons et al. (2013)		This study[a]	
Age	Chron	Begin (Ma)	End (Ma)	Begin (Ma)	End (Ma)	Begin (Ma)	End (Ma)		Begin (Ma)	End (Ma)	Chron	Age (Ma)	Chron	Age (Ma)
	C34n	-	-	125.93	84.19	120.95	-		-	-	C34n	-	C34n	84–121
Aptian	M0r	121.00	120.60	126.30	125.93	121.54	120.95		121.8	-	M0	120.4	M0r	122
Barremian	M1n	123.19	121.00	128.32	126.30	123.51	121.54		123.0	121.8	-	-	-	-
	M1r	123.55	123.19	128.66	128.32	123.92	123.51		123.2	123.0	-	-	-	-
	M2n	124.05	123.55	-	-	-	-		-	-	-	-	-	-
	M3n	-	-	129.11	128.66	124.58	123.92		123.7	123.2	M2	124.1	M3n	124
Barremian	M3r	125.67	124.05	130.60	129.11	126.05	124.58		125.8	123.7	-	-	-	-
	M5n	126.57	125.67	131.43	130.60	127.19	126.05		126.7	125.8	M4	126.7	M5n	126
Hauterivian	M5r	126.91	126.57	131.74	131.43	127.98	127.19		127.0	126.7	-	-	-	-
	M6n	127.11	126.91	131.92	131.74	128.15	127.98		127.1	127.0	M6	127.2	M6n	127
	M6r	127.23	127.11	132.04	131.92	128.33	128.15		127.2	127.1	-	-	-	-
	M7n	127.49	127.23	132.27	132.04	128.54	128.33		127.4	127.2	-	-	-	-
	M7r	127.79	127.49	132.55	132.27	129.00	128.54		127.7	127.4	-	-	-	-
	M8n	128.07	127.79	132.80	132.55	129.32	129.00		128.1	127.7	M8	128.2	M8n	128
	M8r	128.34	128.07	133.05	132.80	129.67	129.32		128.4	128.1	-	-	-	-
	M9n	128.62	128.34	133.30	133.05	130.02	129.67		128.8	128.4	-	-	-	-
	M9r	128.93	128.62	133.58	133.30	130.43	130.02		129.3	128.8	-	-	-	-
	M10n	129.25	128.93	133.88	133.58	130.76	130.43		130.0	129.3	M10	130.5	M10n	130
	M10r	129.63	129.25	134.22	133.88	131.07	130.76		130.5	130.0	-	-	-	-
	M10Nn.1n	129.91	129.63	134.48	134.22	131.35	131.07		130.9	130.5	M10N	131	M10N	131
Hauterivian	M10Nn.1r	129.95	129.91	134.51	134.48	131.47	132.35		131.0	130.9	-	-	-	-
	M10Nn.2n	130.22	129.95	134.76	134.51	131.71	131.47		131.3	131.0	-	-	-	-
Valanginian	M10Nn.2r	130.24	130.22	134.78	134.76	131.83	131.71		131.4	131.3	-	-	-	-
	M10Nn.3n	130.49	130.24	135.00	134.78	132.01	131.83		131.6	131.4	-	-	-	-
	M10Nr	130.84	130.49	135.32	135.00	132.30	132.01		131.9	131.6	-	-	-	-
	M11n	131.50	130.84	135.92	135.32	132.67	132.30		132.5	131.9	M11	132.1	M11n	132
	M11r	131.91	131.50	136.29	135.92	132.99	132.67		132.9	132.5	-	-	M11r	133

[a]Chron ages from geomagnetic time scale of Ogg et al. (2016) adjusted to fit stage and ammonite zone boundary ages of Aguirre-Urreta et al. (2019) complemented with cyclostratigraphy of Bodin et al. (2006) from M1n to M0r and of Martinez et al. (2013) from M10Nn.2n to M11r as shown in Table 2. The base of chron M0r is assigned to the middle of the last ammonite zone of the Barremian stage as indicated by chemo- and biostratigraphic data of Frau et al. (2018), giving an age that corresponds to the youngest age assessed by Olierook, Jourdan et al. (2019) and Olierook, Jiang et al. (2019).

2.2. Structure and Stratigraphy

Extensional structures on the western Australian rifted margin lie west of the Darling Fault, a long-lived structure bordering the western edge of the Archean Yilgarn Craton (Veevers, 2006) (Figure 1). The Perth Basin, a rift basin containing up to 15 km of late Paleozoic, Mesozoic, and Cenozoic strata, lies to the west of the Darling Fault and follows the trend of the older Permian rift system beneath the continental shelf and slope (Harris, 1994; Norvick, 2004; Song & Cawood, 2000; Yeates et al., 1987). On the central part of the margin, the west side of the Perth Basin (Houtman and Zeewyck subbasins) is separated from oceanic crust on the Perth Abyssal Plain by a discontinuous structural high marking the ocean-continent transition zone (Bradshaw et al., 2003). On the southern part of the margin, a structural high underlain by continental crust

Table 2
Revised Hauterivian and Lower Barremian Chron Ages

Chron	Position in ammonite zone (Ogg et al., 2016)	Age at base of ammonite zone (Ma)	Age at top of ammonite zone (Ma)	Revised age at base of chron (Ma)[a]	Gee and Kent (2007) age at base of chron (Ma)	Age difference (m.y.)	Malinverno et al. (2012) age at base of chron (Ma)	Age difference (m.y.)
M0r	50% within Sarasini[b]	122.019	121.519	121.8	121.00	0.8	121.54	0.3
M1n	27% within Sartousiana	123.199	122.339	123.0	123.19	0.2	123.51	0.5
M1r	96% within Vandenheckii	123.999	123.199	123.2	123.55	0.3	123.92	0.7
M3n	38% within Vandenheckii	123.999	123.199	123.7	124.05	0.3	124.58	0.9
M3r	43% within Hugii	126.079	125.539	125.8	125.67	0.1	126.05	0.3
M5n	18% within Ohmi	126.835	126.079	126.7	126.57	0.1	127.19	0.5
M5r	79% within Balearis	127.497	126.835	127.0	126.91	0.1	127.98	1.0
M6n	57% within Balearis	127.497	126.835	127.1	127.11	0.0	128.15	1.1
M6r	42% within Balearis	127.497	126.835	127.2	127.23	0.0	128.33	1.1
M7n	13% within Balearis	127.497	126.835	127.4	127.49	0.1	128.54	1.1
M7r	63% within Ligatus	128.145	127.497	127.7	127.79	0.1	129.00	1.3
M8n	11% within Ligatus	128.145	127.497	128.1	128.07	0.0	129.32	1.2
M8r	69% within Sayni	129.099	128.145	128.4	128.34	0.1	129.67	1.3
M9n	30% within Sayni	129.099	128.145	128.8	128.62	0.2	130.02	1.2
M9r	74% within Nodosoplicatum	129.992	129.099	129.3	128.93	0.4	130.43	1.1
M10n	97% within Loryi	130.520	129.992	130.0	129.25	0.8	130.76	0.8
M10r	9% within Loryi	130.520	129.992	130.5	129.63	0.9	131.07	0.6
M10Nn.1n	49% within Radiatus	131.292	130.520	130.9	129.91	1.0	131.35	0.4
M10Nn.1r	40% within Radiatus	131.292	130.520	131.0	129.95	1.1	131.47	0.5
M10Nn.2n	89% within Furcillata	131.935	131.292	131.4	130.22	1.2	131.71	0.3
M10Nn.2r	86% within Furcillata	131.935	131.292	131.4	130.24	1.2	131.83	0.4
M10Nn.3n	51% within Furcillata	131.935	131.292	131.6	130.49	1.1	132.01	0.4
M10Nr	Base Furcillata	131.935	131.292	131.9	130.84	1.1	132.30	0.4
M11n	59% within Peregrinus	133.393	131.935	132.5	131.50	1.0	132.67	0.2
M11r	34% within Peregrinus	133.393	131.935	132.9	131.91	1.0	132.99	0.1

[a]Revised chron ages are interpolated from position of chron from base of reference ammoniate zone and ages of ammonite zone (Ogg et al., 2016) using revised stage ages of Aguirre-Urreta et al. (2019) complemented with cyclostratigraphy of Bodin et al. (2006) from M1n to M3n and cyclostratigraphy of Martinez et al. (2013) from M10Nn.2n to M11r. Geomagnetic time scales of Gee and Kent (2007) and Malinverno et al. (2012) shown for comparison. [b]The biostratigraphic position of chron M0r was revised in Frau et al. (2018). The age given here assumes the base of this chron is in the middle of the Sarasini Zone.

(the Yallingup Shelf) borders the west side of the Perth Basin, separating it from the deep water Mentelle Basin (Figure 1).

Seismic reflection profiles image a breakup unconformity in the Mentelle Basin that is similar to the widespread breakup unconformity drilled in the Perth Basin and has been inferred to be of similar (Valanginian) age (Figure 3) (Borissova, 2002; Borissova et al., 2010; Bradshaw et al., 2003; Maloney et al., 2011). The eastern Mentelle Basin, located beneath the continental slope in water depths of 500–2000 m, contains up to 1 km of postrift sedimentary strata above the unconformity that thins and onlaps onto the western side of the Yallingup Shelf (Figure 3a). Strata below the seismically imaged breakup unconformity in the eastern Mentelle Basin are heavily extensionally faulted, as in the Perth Basin. The western Mentelle Basin lies in water depths of 2,000–4,000 m and contains up to 2.7 km of postrift strata that onlap and cover the eastern flank of the Naturaliste Plateau (Figures 3b and 3c). The western Mentelle Basin contains fewer faults than the eastern Mentelle Basin, but abundant volcanic features on top of the breakup unconformity that
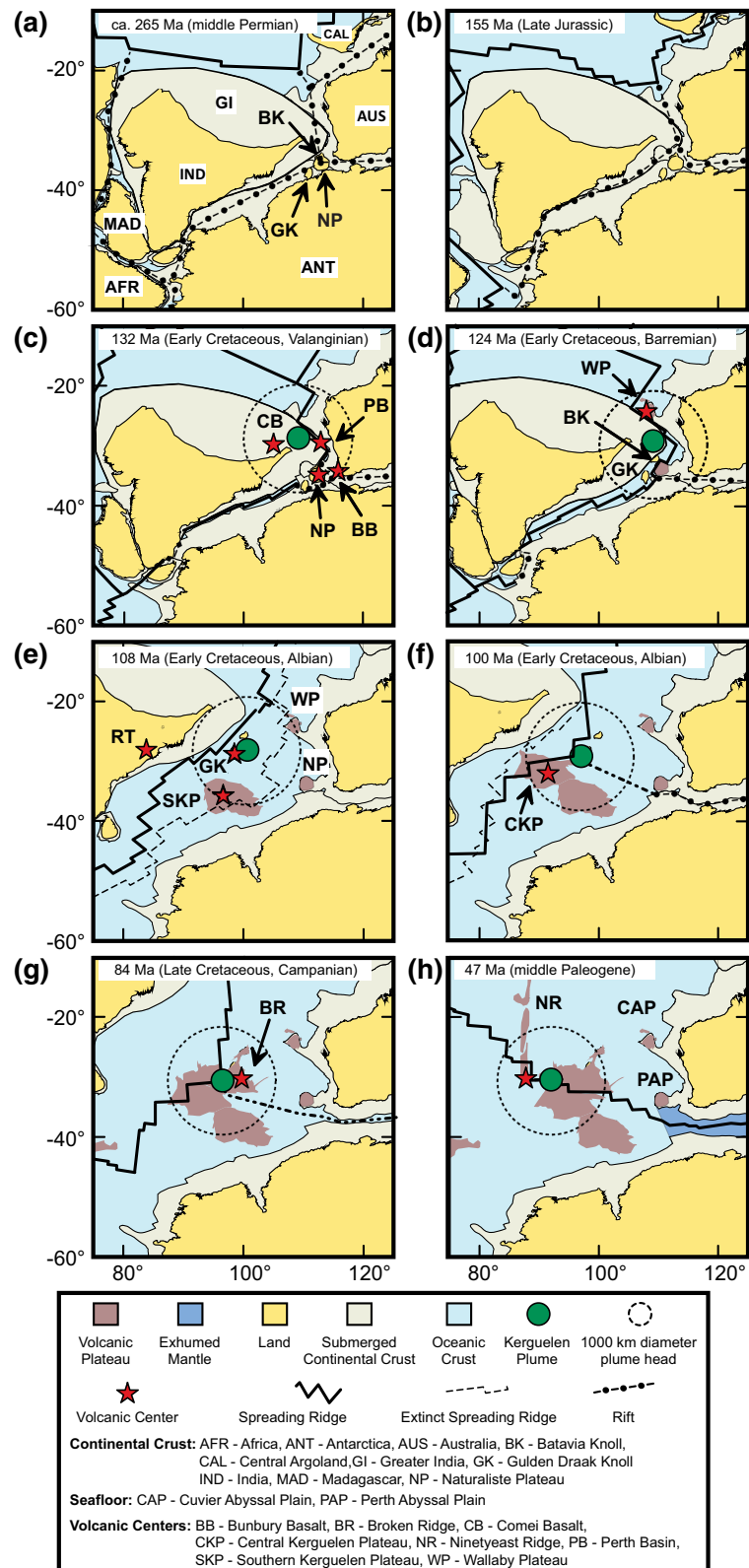
are similar to features imaged on seismic data from the main part of the Naturaliste Plateau further west (Borissova, 2002). Seismic reflection data show several rift basins beneath the unconformity on the Naturaliste Plateau and in the western Mentelle Basin that are filled with divergent dipping reflectors suggestive of either siliciclastic or volcanic/volcaniclastic growth strata (Borissova, 2002; Hall et al., 2013; Maloney et al., 2011), but these strata have not been drilled.

Basement rocks dredged from the southern Naturaliste Plateau include Mesoproterozoic metasedimentary rocks and orthogneiss that have been correlated with similar rocks exposed in the Albany-Fraser-Wilkes orogen onshore on the southern Australian margin and the conjugate Antarctica margin (Halpin et al., 2008, 2020) (Figure 1). Mafic clasts recovered from dredge hauls on the north and south margins of the plateau, volcaniclastic strata drilled above the breakup unconformity at Deep Sea Drilling Project (DSDP) Sites 258 and 264 (located on the northeastern and southern margins of the plateau, respectively) and seismic profiling have shown the basement of the plateau is capped with basaltic rocks that are similar in age and geochemical characteristics to the Bunbury Basalt that outcrops onshore and has been drilled in the southern Perth Basin (Coleman et al., 1982; Direen et al., 2017). Gravity models indicate the thickness of the crust (including the syn- and postrift sediments) is more than 35 km beneath the Yilgarn craton, 30–35 km beneath the Yallingup Shelf, 20–25 km in the Perth Basin, 18–20 km on the Naturaliste Plateau, and about 17 km in the northern Mentelle Basin (Direen et al., 2007; Olierook et al., 2016). Gravity models permit that the crystalline crust in the western Mentelle Basin (excluding postrift strata) may be less than 5 km thick (Johnston et al., 2010). Assuming a prerift crust thickness similar to that on the Yallingup Shelf or Yilgarn Craton (30–35 km), the corresponding extension factors are $\beta \approx 1.4$–1.6 on the Naturaliste Plateau and in the Perth Basin and $\beta \approx 3$ beneath the central Mentelle Basin (Olierook et al., 2016).

2.3. Magmatism and the Role of the Kerguelen Plume

Continental breakup in the eastern Indian Ocean was accompanied by mafic volcanism between 137 and 130 Ma in the southern Perth Basin (exposed onshore as the Bunbury Basalt) (Olierook et al., 2016) and between at least 131 and 128 Ma on the Naturaliste Plateau (Direen et al., 2017; Olierook et al., 2017). Seismic reflection data show volcanic edifices and flows atop the breakup unconformity on most of the Naturaliste Plateau and throughout the western Mentelle Basin, and seaward dipping reflectors interpreted to be volcanic flows have been imaged near the ocean-continent boundary in the northern Perth Basin and on the margin of the Wallaby Plateau (Borissova, 2002; Bradshaw et al., 2003; Colwell et al., 1994; Goncharov & Nelson, 2012; Owens et al., 2018; Norvick, 2004; Symonds et al., 1998). Similar age basalts are present on the conjugate Greater Indian margin, now exposed in southern Tibet (the 140–130 Ma Comei basalts; Liu et al., 2015; Zhou et al., 2017; Zhu et al., 2009). Based on spatial proximity and trace element and isotopic similarities, the Bunbury Basalt, Naturaliste Plateau basalts, and Comei basalts have been inferred to be petrogenetically related to younger basalts produced by the Kerguelen mantle plume on the Wallaby Plateau (124 Ma) (Olierook et al., 2015), eastern Indian margin (the 118 Ma Rajmahal Traps and Cona Basalts) (Baksi, 1995; Baksi et al., 1987; Ingle et al., 2004; R. W. Kent et al., 2002; D. Zhu et al., 2008), and Kerguelen Plateau (>119–100 Ma) (Coffin et al., 2002; Duncan, 2002; Frey et al., 2000; Ingle et al., 2002; Mahoney et al., 1995; Whitechurch et al., 1992). The presence of a ca. 1,000 km diameter Kerguelen plume head beneath the lithosphere at the time of breakup has been proposed to account for the broad paleogeographic

Figure 2. Opening of the southeastern Indian Ocean. Plate reconstructions from GPlates based on the plate model of Gibbons et al. (2013) and geomagnetic time scale in Table 1. Extent of Greater India and location of Kerguelen plume from Gibbons et al. (2012). (a) Middle Permian—extension along the margins of the East Gondwana continents. (b) Late Jurassic—renewed extension along the Permian rift trend. (c) Late Valanginian—seafloor spreading begins between India and Antarctica and in the Perth Abyssal Plain between Greater India and Australia. Volcanism in the southern Perth Basin (130–137 Ma Bunbury Basalt; Olierook et al., 2016), near the ocean-continent transition in the northern Perth Basin, in the western Mentelle Basin and on the Naturaliste Plateau (128–132 Ma; Direen et al., 2017), and on the conjugate Greater Indian margin (140–130 Ma Comei Basalts; Zhou et al., 2017). (d) Early Barremian—shortly after seafloor spreading begins between Greater India and the Naturaliste Plateau, coeval with volcanism on the Wallaby Plateau (124 Ma; Olierook et al., 2015). (e) Albian—a ridge jump transfers Gulden Draak and Batavia Knolls to the Australia-Antarctica plate. Volcanism was underway on the southern Kerguelen Plateau (118–119 Ma; Coffin et al., 2002; Duncan, 2002), on the conjugate Indian margin (Rajmahal Traps, 118 Ma; Ingle et al., 2004; R. W. Kent et al., 2002) and on Gulden Draak Knoll (117 Ma; Whittaker et al., 2016). (f) Albian—India begins to move northward after reorientation of the Southeast Indian Ridge. Extension between Australia and Antarctica and volcanism on the central Kerguelen Plateau and Broken Ridge begins. (g) Late Cretaceous—Mantle exhumation and/or slow seafloor spreading begins between Antarctica and Australia ca. 85 Ma. Continued Kerguelen hotspot volcanism begins to construct the Ninetyeast Ridge. (h) Paleogene—normal seafloor spreading begins between Australia and Antarctica.
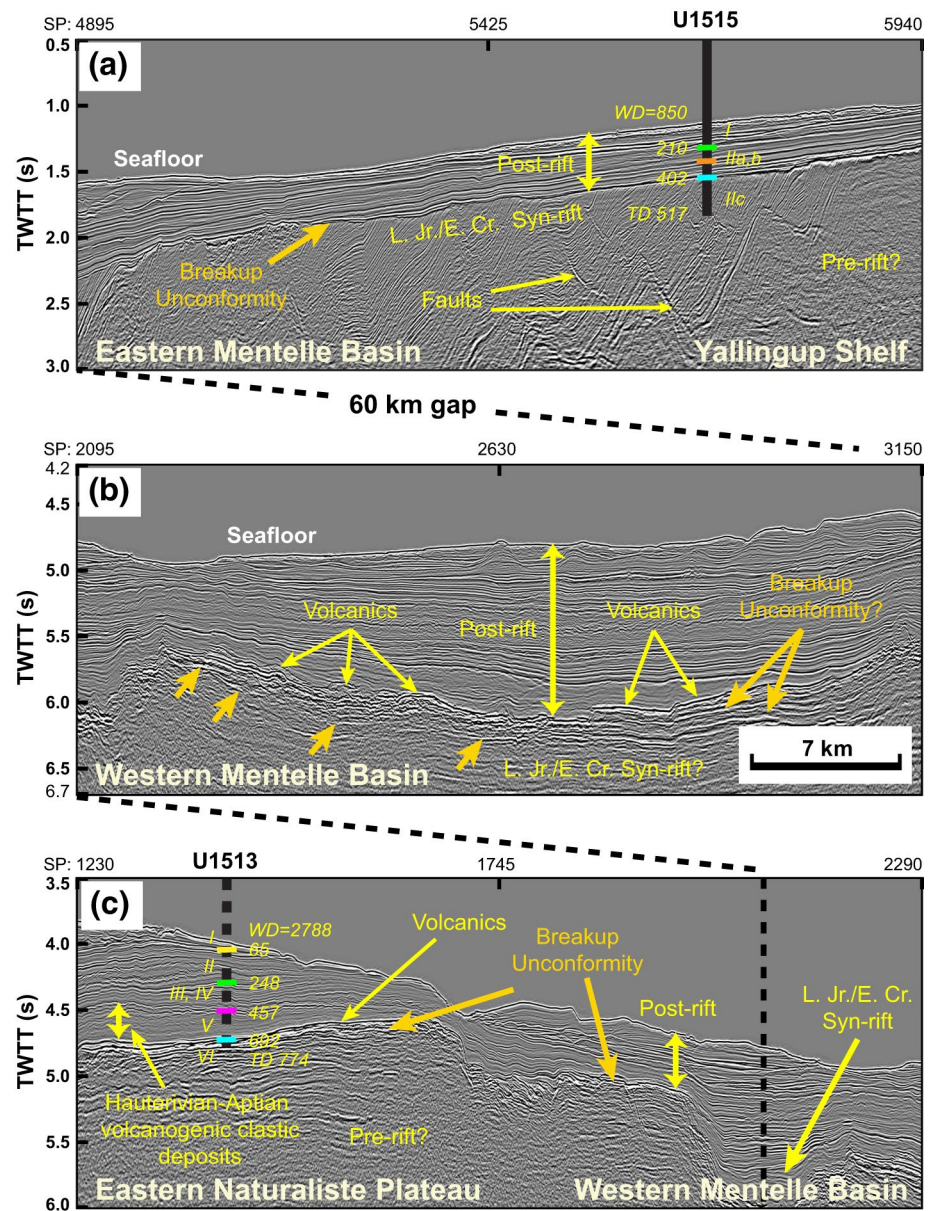
Figure 3. Portions of seismic reflection profile S310-05 showing structural and stratigraphic characteristics of the southwestern Australian continental margin. Seismic sections align at edges as indicated by dotted lines to form a single profile, with 60 km gap between (a) and (b) and 7 km overlap between (b) and (c). (a) Portion of the eastern part of the profile crossing Yallingup Shelf and eastern Mentelle basin showing location of International Ocean Discovery Program (IODP) Site U1515. Solid vertical line shows Hole U1515A, with colored bars indicating boundaries between lithostratigraphic units discussed in text (roman numerals). (b) Portion of the central part of the seismic profile, crossing deep water western Mentelle Basin. (c) Portion of the western part of the seismic profile, crossing western edge of Mentelle Basin and eastern flank of the Naturaliste Plateau. Locations of IODP Site U1513 and DSDP Site 258 (not distinguishable from Site U1513 on this projection) are projected along structural strike from 20 km to the south. WD, water depth in meters; other numbers indicate depth below seafloor. Locations shown in Figure 1. Seismic profile is available from Geoscience Australia National Offshore Petroleum Information Management System (https://nopims.dmp.wa.gov.au/nopims). Seismic interpretation is modified after Hall et al. (2013), updated with IODP Expedition 369 drilling results using the time-depth conversions published in the Expedition 369 Proceedings for Sites U1513 (Huber et al., 2019a) and U1515 (Huber et al., 2019b).

distribution of these basalts (Figure 2c) (Direen et al., 2017; Frey et al., 1996; Ingle et al., 2002, 2004; R. W. Kent et al., 2002; Olierook et al., 2016, 2017; Storey et al., 1989; Zhou et al., 2017; Zhu et al., 2009). However, other models for petrogenesis of the basalts emplaced around the Indian Ocean during rifting and breakup have also been proposed. Regional contamination of the asthenospheric mantle by the broad Kerguelen plume head has been suggested to have increased the fertility and enriched the isotopic and trace element compositions of the mantle prior to rifting, perhaps creating an antecedent plume-like reservoir that was tapped at various times and places during rifting (R. Kent, 1991; Storey et al., 1989). Alternatively, the Kerguelen plume may have fragmented or segregated into spatially distinct rising limbs, thus accounting for the broad and irregular distribution of the volcanic rocks (Coffin et al., 2002). Lastly, isotopic data suggesting a mixture of both depleted and enriched sources have been interpreted to indicate derivation from sources in the depleted asthenospheric mantle combined with either sublithospheric mantle (Olierook et al., 2016) or lithospheric mantle (Olierook, Jiang et al., 2019) that was enriched in incompatible elements during the Late Proterozoic assembly of East Gondwana. Thus, the relationship between plumes and Early Cretaceous basalts in the eastern Indian Ocean remains uncertain. Opening of the Southern Ocean between Australia and Antarctica in Late Cretaceous through Paleogene time appears to have been amagmatic prior to the onset of seafloor spreading (Direen et al., 2011).

3. Findings From IODP Expedition 369

IODP Expedition 369 drilled one site at the western edge of the Mentelle Basin above the eastern flank of the Naturaliste Plateau (Site U1513), two sites in the central Mentelle Basin (Sites U1514 and U1516), and one site in the eastern Mentelle Basin near the Yallingup Shelf (Site U1515) (Hobbs et al, 2019; Huber et al., 2018) (Figure 1). Key outcomes of the expedition were recovery of (i) strata spanning the breakup unconformity in the eastern Mentelle Basin; (ii) the first samples of in situ basalts on the Naturaliste Plateau, which provide new constraints on the thermal state of the mantle during rifting; (iii) a complete clastic succession containing weathered volcanic material deposited on the Naturaliste Plateau between the Perth Abyssal Plain and Naturaliste Plateau breakup events; and (iv) nearly complete postbreakup successions on the Naturaliste Plateau and in the Mentelle Basin, which provide new constraints on the subsidence history of the southwestern Australian margin.

IODP Hole U1515A was drilled to a depth of 517 m below seafloor (mbsf) in 850 m of water on the eastern margin of the Mentelle Basin, on the continental rise adjacent to the Yallingup Shelf (Figures 1 and 3a). Two lithostratigraphic units were identified (Figure 4). Unit I consists of a Pleistocene to upper Campanian or upper Santonian dominantly ooze, chalk, chert, and limestone sequence encountered in the upper 129 m of the hole. Benthic foraminifera indicate deposition in bathyal water depths (200–2000 m) for most of unit I, with outer neritic (up to 200 m) to upper bathyal (200–600 m) depths in the uppermost part of the unit. An interval of poor recovery across a detachment surface separates unit I from glauconitic sandstone, sand, and silty sand in lithostratigraphic unit IIa between 210 and 325 mbsf. A 10 m interval of poor recovery separates unit IIa from unit IIb. At its top, unit IIb is dominantly sandstone with interbedded siltstone and claystone that is distinguished from unit IIa by the presence of pyrite and less abundant glauconite. Unit IIb transitions downward across a poorly recovered boundary between 376 and 402 mbsf into lithostratigraphic unit IIc, which is an organic-rich silty sandstone and claystone containing coal, plant debris, fern pollen, freshwater algae, and possible indicators of dinoturbation. Palynomorphs indicate an earliest Cretaceous (Valanginian or younger) age for lithostratigraphic unit IIb and a Late Jurassic (Kimmeridgian to Tithonian) age for unit IIc (Wainman et al., 2020). Unit IIc is interpreted to have been deposited in a fluvio-lacustrine environment in the upper part of the synrift strata filling one of several small fault bounded basins imaged on seismic data in the eastern Mentelle Basin (Figure 3a). Unit IIb is interpreted to be nearshore facies deposited on a subsiding coast, with increasing marine incursions near the top that culminated in deposition of the glauconitic sandstone in unit IIa. A prominent reflector from the boundary between lithostratigraphic units IIc and IIb at Site U1515 can be traced into the western Mentelle Basin, where it manifests as an undated unconformity below the basalt flows at the top of the faulted synrift strata (Figure 3c).

IODP Sites U1514 (water depth 3,850 m) and U1516 (2,675 m) are respectively located in the northern and southern parts of the central Mentelle Basin, where the basin is structurally and bathymetrically deep-
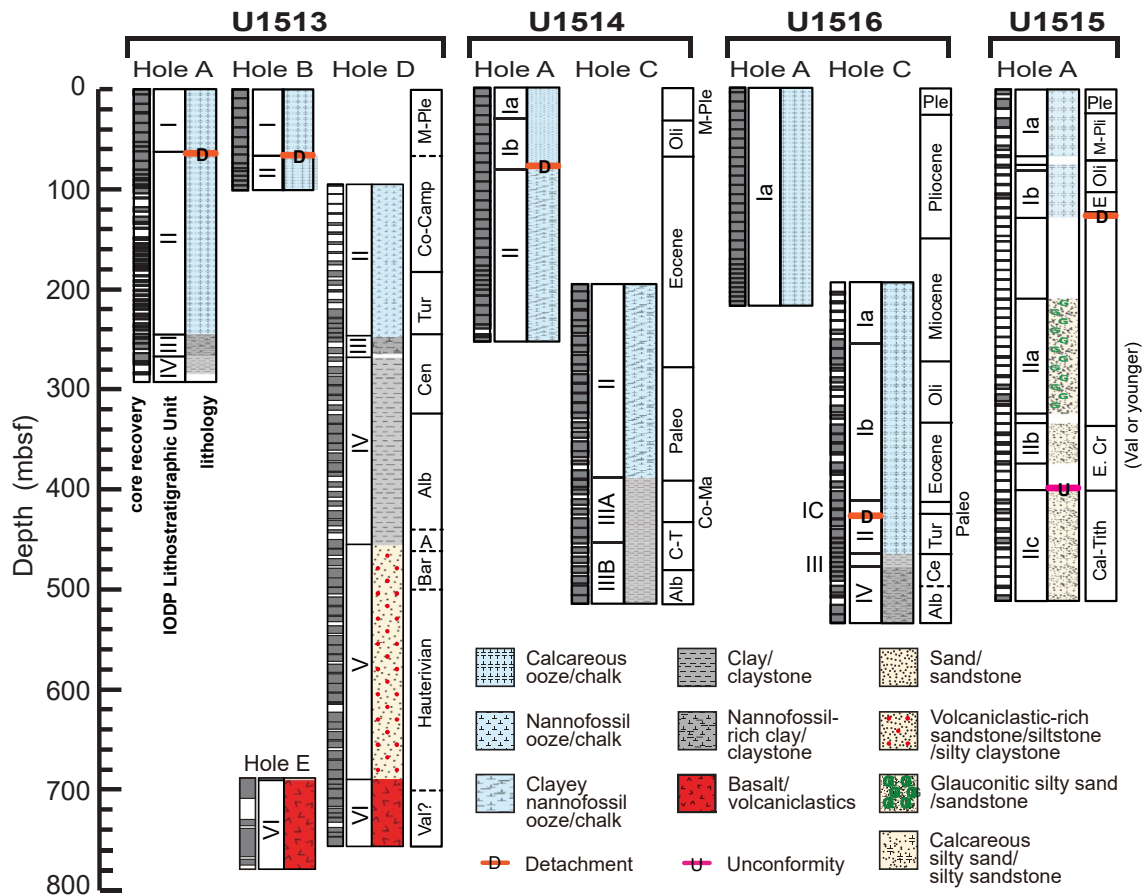
Figure 4. Stratigraphic columns for International Ocean Discovery Program boreholes in the Mentelle Basin. Boreholes are arranged from west to east (white indicates no recovery). Compiled from Hobbs et al. (2019).

est (Figure 1). Drilling at both sites encountered up to 400 m of Pleistocene to Miocene or late Eocene ooze (lithostratigraphic unit I) overlying Eocene to Paleocene chalk that grades downward into claystone (lithostratigraphic unit II at Site U1514, and subunits Ib and Ic at Site U1516) (Figure 4). At Site U1514, lithostratigraphic unit II conformably overlies a Paleocene through Albian claystone and silty claystone (unit III). At Site U1516, a detachment separates the base of the Paleocene claystone (subunit Ic) from an underlying Turonian cherty chalk and claystone (unit II). Unit II conformably overlies a Cenomanian through Albian succession of chalk and claystone (units III and IV). Benthic foraminifera indicate middle bathyal (600–1,000 m) to lower bathyal (1,000–2000 m) water depths for deposition of units I and II, and bathyal water depths for unit III at Site U1514. Bathyal water depths are indicated throughout the succession cored at Site U1516.

IODP Site U1513 is located at 2,788 m water depth on the western edge of the Mentelle Basin, overlying the eastern margin of the Naturaliste Plateau (Figures 1 and 3c). Six lithostratigraphic units are identified in a composite stratigraphic section created from five clustered boreholes, extending to a maximum depth of 774 mbsf (Figure 4). The upper 65 m of strata consists of Pleistocene through late Miocene dominantly calcareous ooze (lithostratigraphic unit I). A depositional hiatus associated with a hardground separates unit I from an underlying 181 m thick Cenomanian through Campanian calcareous ooze and chalk interval (lithostratigraphic unit II). Benthic foraminifera indicate bathyal and middle bathyal water depths for deposition of units I and II, respectively. Unit II is underlain by a 209 m thick Cenomanian through Albian clay and claystone deposited in middle bathyal to bathyal water depths (lithostratigraphic unit III, 22 m thick; and unit IV, 187 m thick). The clay and claystone beds conformably overlie a 235 m thick lithic-rich clayey siltstone and sandstone interval ranging from early Aptian to earliest Hauterivian in age that contains
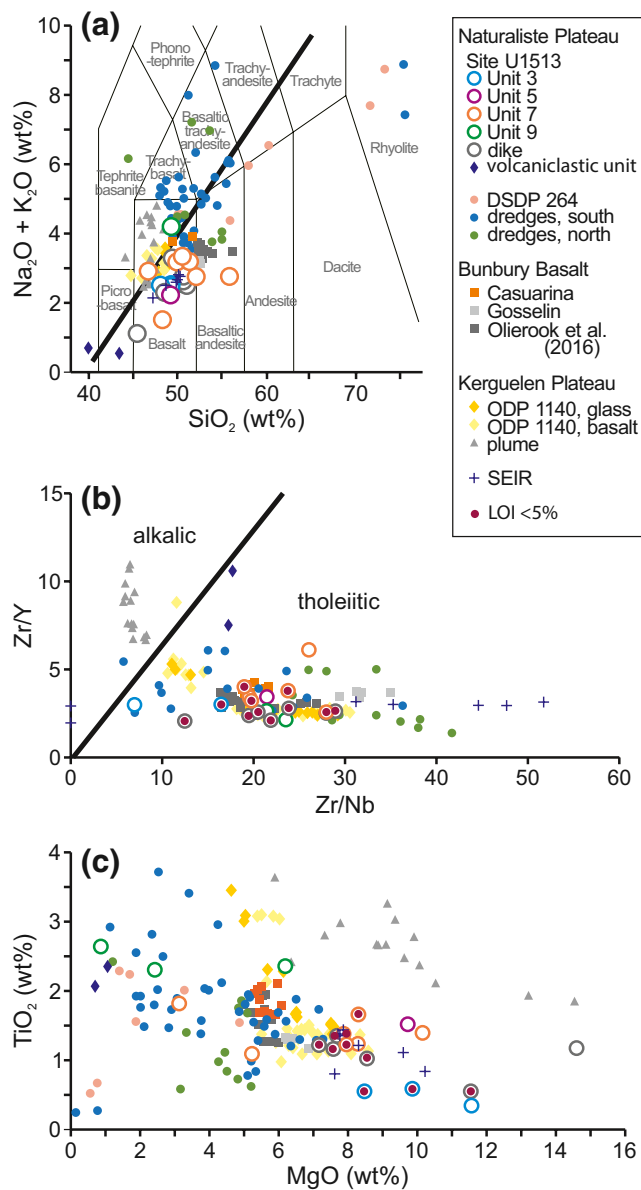
Figure 5. Major element binary plots and trace element ratio plots for volcanic rocks and dikes recovered from volcanic unit VI at International Ocean Discovery Program Site U1513 (data from Huber et al., 2019a, 2019b). Shown for comparison are data for dredged basaltic rocks from the Naturaliste Plateau (Coleman et al., 1982; Direen et al., 2017; Ford, 1975; Mahoney et al., 1995; Storey et al., 1992), Bunbury Basalt (Direen et al., 2017; Frey et al., 1996; Olierook et al., 2016), and Kerguelen Plateau basalts (Doucet et al., 2005; Frey et al., 2000; Kurnosov et al., 2003; Wallace, 2002; Weis & Frey, 2002). (a) Total alkali versus silica, showing basaltic composition of Site U1513 mafic rocks (classification diagram after Le Bas et al., 1986). (b) Representative trace element composition, showing Site U1513 and Kerguelen Plateau basalts to lie along a mixing trend between the Southeast Indian Ridge and Kerguelen plume basalts. (c) Major element composition, showing overlap with Kerguelen Plume, Southeast Indian Ridge, and Kerguelen Plateau basalts. High-MgO basalts are used for petrogenetic modeling as described in the text.

glauconite, pyrite, shell fragments, plant debris, and abundant volcanic mineral grains and clasts (lithostratigraphic unit V) (Huber et al., 2019a, 2019b; Lee et al., 2020). A similar lithostratigraphic unit, rich in volcanic clasts and with a ferruginous detrital claystone at its base, was encountered at nearby DSDP Site 258 (Davies et al., 1974). These strata are interpreted to be epiclastic deposits comprised primarily of material weathered from nearby (but perhaps not immediately local) volcanic sources. Unit V matches the definition of secondary (epiclastic) volcaniclastic deposits used by many authors (Fisher, 1961; Mulder, 2011), but more recent usage has excluded epiclastic deposits from the volcaniclastic classification (Manville et al., 2009; McPhie et al., 1993). Following the more recent usage, we refer to unit V in this study as a volcanogenic clastic, or simply an epiclastic succession. Taken together, the sedimentary structures, trace fossils, benthic foraminifera, and palynomorphs indicate deposition in shallowing water depths downward in the section from upper bathyal to neritic for unit V. An 83 m thick interval of interbedded basalt flows and volcaniclastic flows recording at least five eruption episodes (lithostratigraphic unit VI) lies below unit V, but the total thickness of unit VI is undetermined (Figure 4) (Huber et al., 2019a, 2019b; Tejada et al., 2020). The entire volcanic and volcanogenic clastic interval (units VI and V) was hydrothermally altered prior to deposition of unit IV, but the least (weakly to moderately) altered samples from unit VI have SiO_2 contents (43.7–52.5 wt%), total alkali contents (2.11–2.38 wt%), and Zr/Y and Zr/Nb ratios typical of tholeiitic basalts (Figures 5a and 5b). The unit VI flows with the lowest total alkali contents appear to be less altered than either the Bunbury Basalt or other mafic rocks recovered by previous dredging on the Naturaliste Plateau (Figures 5a and 5c). The basalt flows in unit VI are undated, but the magnetostratigraphic age of unit V spans chrons M10Nn.1n to M0r (131–121 Ma) (Huber et al., 2019a, 2019b; Lee et al., 2020). The underlying basalt flows of unit VI thus predate the end of chron M10Nn.1n. This gives a minimum age of 131 Ma (earliest Hauterivian) for their emplacement, indicating that the flows were likely contemporaneous with the Bunbury Basalt eruptions (130–137 Ma; Olierook et al., 2016).

4. Analysis: New Constraints on Breakup, Basalt Petrogenesis, Extension, and Subsidence

4.1. Stratigraphic Record of the Rift to Drift Transition on the Southwest Australian Margin

The basalt flows of lithostratigraphic unit VI at Site U1513 lie on top of the breakup unconformity imaged in seismic reflection data (Figure 3c), as envisioned by Maloney et al. (2011). The seismic unconformity can be traced into the eastern Mentelle Basin where it is equivalent or nearly equivalent to the Valanginian breakup unconformity encountered at Site U1515. Pillow structures present in some flows and oxidation of most flows suggest eruption in a nearshore shallow water to subaerial environment (Huber et al., 2019a; Tejada et al., 2020). We interpret the basalt flows to have been erupted near sea level during the last stages of extension on this part of the southwestern Australian margin, immediately after seafloor spreading had begun on the Perth Abyssal Plain between magnetochrons M11r and M11n (133–132 Ma) but before the onset of seafloor spreading west of the Naturaliste Plateau between magnetochrons

M5n and M3n (126–124 Ma). The overlying epiclastic sequence of unit V contains volcanic mineral grains and lithic fragments interpreted to be eroded from volcanic rocks on the Naturaliste Plateau or perhaps further south on the conjugate Antarctica margin, which were reworked and deposited in shallow marine to upper bathyal conditions (Lee et al., 2020) as the Perth Abyssal Plain spreading center migrated westward along the northern margin of the plateau. A similar interpretation was made of the volcaniclastic strata encountered at nearby DSDP Site 258 (Davies et al., 1974). The breakup unconformity imaged on seismic data below the basalt flows is thus interpreted to be associated with the onset of seafloor spreading on the Perth Abyssal Plain, in keeping with previous interpretations (Borissova et al., 2010; Hall et al., 2013). If anomaly M11n is accepted as the oldest seafloor spreading anomaly on the Perth Abyssal Plain (Markl, 1974; Robb et al., 2005), then breakup must have occurred after chron M11r (133 Ma, Table 1). As noted in Section 3, the basalt flows encountered above the breakup unconformity at IODP Site U1513 must predate chron M10Nn.1n (131 Ma). This implies a narrowly constrained and approximately coeval age of 132–133 Ma for the Perth Basin breakup event and emplacement of the Site U1513 basalts.

The onset of seafloor spreading west of the Naturaliste Plateau (the Naturaliste Plateau breakup event) occurred during deposition of the upper part of lithostratigraphic unit V. We associate this breakup event with a conformable upward transition from clayey siltstone (subunit 3) to silty claystone (subunit 2) and corresponding decreases in the abundance of fossils, bioturbation, and volcanic material (Huber et al., 2019a, 2019b; Lee et al., 2020). Benthic foraminifera indicate deepening of the seafloor from neritic to upper bathyal depths during this interval, followed by subsidence to at least middle bathyal water depth during Aptian time between deposition of unit V and the marine claystones of unit IV. The transition between subunits 2 and 3 is near the boundary between chrons M5n and M3r (Lee et al., 2020), indicating an age of 126 Ma (Table 1) for the Naturaliste Plateau breakup event (in agreement with the age range indicated by the seafloor spreading anomalies).

### 4.2. Constraints on Melting Conditions for the Naturaliste Plateau Basalts

Several of the basalt flows from Site U1513 have relatively high MgO (8.7–11.8 wt%) and low TiO_2 (0.31–0.60 wt%) contents that are respectively suggestive of relatively high degrees of melting and low degrees of fractionation. These primitive composition basalts (MgO > 8 wt%) provide the first constraints on melting conditions and primary magma composition for Naturaliste Plateau volcanic rocks. Petrogenetic modeling based on major element data from the least altered high-MgO sample, using PRIMACALC_2.10 with CO-MAGMAT3.72 (Kimura & Ariskin, 2014), indicates a primary magma composition with Mg# = 0.77 and equilibrium olivine forsterite content Fo = 92%. This primary magma can be generated from approximately 25% melting of a lherzolite source at 1.5 GPa (approximately 50 km depth), with modeled magmatic temperatures of 1369°C–1413°C (Figure 6, Table 3). These magmatic temperatures are equivalent to mantle potential temperatures of 1380°C–1410°C, with a nominal value of 1400°C, estimated using (Ocean Basalt Simulator Version 1 [OBS1]; Kimura & Kawabata, 2015). Except for the most altered samples (LOI > 5 wt%), the major element and trace element compositions of the Site U1513 basalts overlap with the compositional fields of basalts encountered at ODP Site 1,140 on the Kerguelen Plateau (e.g., Figures 5b and 5c). The origin of the Site 1,140 basalts has been interpreted to be mixing of Kerguelen plume and Southeast Indian Ocean Ridge depleted mantle sources (Dosso et al., 1988; Wallace et al., 2002; Weis & Frey, 2002). We infer a similar origin for the Naturaliste Plateau basalts.

4.3. Crustal Thinning and the Amount and Distribution of Extension

Paleo drainage patterns determined from detrital zircons indicate that the western Australian margin was a relatively flat peneplain in Early Jurassic time (Sircombe & Freeman, 1999). Assuming Airy isostasy, a prerift elevation at sea level, and postrift thermal reequilibration of the rifted lithosphere, the minimum amount of thinning of the crust, ΔH, can be determined from the present depth of the breakup unconformity:

$$\Delta H = WD \frac{(\rho_m - \rho_w)}{(\rho_m - \rho_c)} + ST \frac{(\rho_m - \rho_s)}{(\rho_m - \rho_c)}$$

(1)
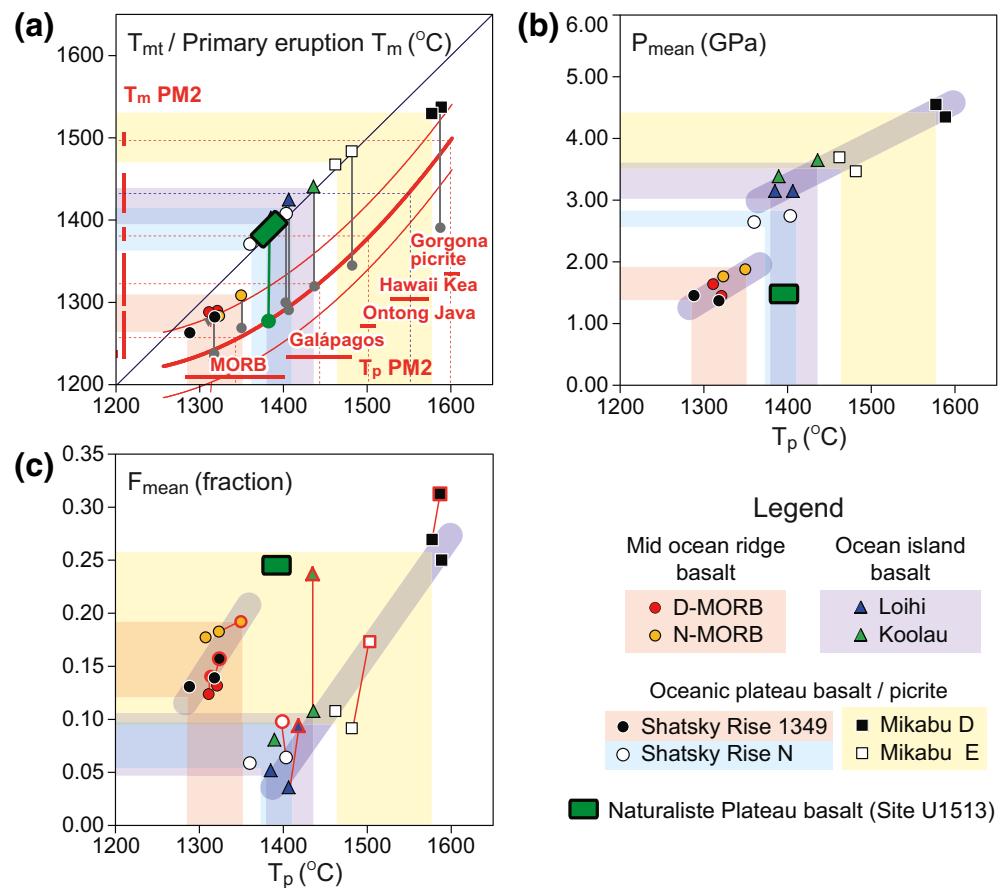
Figure 6. Modeled potential temperature (T_p) versus melting temperature, melting pressure, and degree of melting for mid-ocean ridge basalts, ocean island basalts, and oceanic plateau basalts and picrites obtained from the Ocean Basalt Simulator Version 1 (OBS1) petrogenetic model (adapted from Kimura & Kawabata, 2015). Symbols show OBS1 models for locations indicated in the legend. The green box shows modeling results for International Ocean Discovery Program Site U1513 basalts (this study). (a) Modeled melting temperature at the termination of melting (T_{mt}) as a function of mantle potential temperature (T_p). Gray circles and vertical bars indicate corresponding mantle solidus temperature (T_m) at the mean melting pressure estimated from the OBS1 models. Horizontal and vertical red lines labeled PM2 indicate T_p and T_m at the olivine liquidus estimated using PRIMELTS2 (Herzberg & Asimow, 2008; Herzberg et al., 2007) for the indicated eruptive centers. Shaded areas indicate nominal ranges. Thick red curved line indicates T_m–T_p correlation curve, with thin red lines indicating range. (b) Modeled mean melting pressure as a function of T_p. Shaded bars illustrate correlations within tectonic settings. (c) Mean melt fraction as a function of T_p. Symbols with red outlines indicate melt mixing trends as discussed by Kimura and Kawabata (2015).

where WD is water depth (2,788 and 850 m at Sites U1513 and U1515, respectively), ST is strata thickness above the unconformity (∼800 and 335 m), and ρ_m, ρ_c, ρ_s, and ρ_w are the densities of the mantle (3,300 kg m^{-3}), crust (2,800 kg m^{-3}), postrift strata (2,300 kg m^{-3}), and water (1,000 kg m^{-3}) (e.g., Lee et al., 2019). This indicates that the crust has been thinned by at least 14 and 5 km at Sites U1513 and U1515, respectively. The thickness of the crust prior to extension is unknown, but is likely to have been similar to the unextended crust beneath either the Yilgarn Craton east of the Perth Basin onshore, or the relatively unextended Yallingup Shelf that lies between the Perth and Mentelle Basins. Gravity, seismic refraction, and receiver function studies show the thickness of the crust in the western Yilgarn Craton typically ranges between 32 and 38 km, and may locally be as thick as 43 km (Dentith et al., 2000; B. L. N. Kennett et al., 2011; Olierook et al., 2016; Reading et al., 2003; Saygin & Kennett, 2012). The thickness of the crust beneath the Yallingup Shelf is similar to that of the craton, ranging from 30 to 35 km (Direen et al., 2007; Olierook et al., 2016). Taking the extremes (30 and 43 km) as indications of the prerift crust thickness suggests that the crust has been thinned a minimum of 33%–44% at Site U1513 in the western Mentelle Basin, and by 12%–16% at Site U1515 in the eastern Mentelle Basin. If thinning is attributed entirely to extension, the cor-

Table 3
*Petrogenetic Modeling Input Parameters and Results*

Major elements	Sample 67R-01W measured composition (wt %)[a]	Modeled magma chamber composition (wt %)	Modeled primary basalt magma composition (wt %)
SiO_2	49.11	49.09	48.54
TiO_2	0.54	0.53	0.50
Al_2O_3	18.99	18.97	17.63
FeO	7.76	7.78	7.79
MnO	0.16	0.15	0.15
MgO	11.66	11.67	14.44
CaO	9.41	9.40	8.73
Na_2O	2.31	2.32	2.15
K_2O	0.03	0.03	0.03
P_2O_5	0.04	0.05	0.04
SUM	100.00	100.00	100.00
Other key compositional indicators		Modeled magma chamber	Modeled primary basalt
Ni content of olivine (wt%)		0.35	0.49
Forsterite content of olivine (wt%)		91.0	91.9
Mg# of basalt		0.73	0.77
FeO/Fe_2O_3(total) ratio		0.87	0.89
Water content (wt%)		0.00	0.01
Modeled melting conditions		Modeled magma chamber	Modeled primary basalt
Magma temperature using method of Ariskin (1999) (°C)		1,296	1,369
Magma temperature using method of Kimura and Ariskin (2014) (°C)		-	1,413
Magma temperature using method of Herzberg and Asimow (2008) (°C)		-	1,413
Modeled mantle potential temperature (°C)		-	1,380–1,410
Melting pressure (GPa)		0.00	1.5
Degree of melting		-	24.8
Degree of fractionation		-	10

[a]Based on X-Ray Fluorescence analysis using AXIOS Plus (Panalytical) instrument at University of Oldenburg on shipboard residual sample powder previously analyzed by inductively coupled plasma-atomic emission spectrometry (Huber et al., 2019a).

responding extension factors are β = 1.5–1.8 at Site U1513 and β = 1.1–1.2 at Site U1513. Similar amount of extension, β = 1.4–1.6, were estimated by Olierook et al. (2016) for the southern Perth Basin and the Naturaliste Plateau, although they estimate higher values (β = 3) in the central Mentelle Basin. However, it need be recognized that additional alterations of the crust thickness, beyond extensional thinning, likely occurred during rifting and affected the isostatic state of the margin. Specifically, some portion of crust thinning was likely accommodated by erosion during uplift in the early stages of rifting (e.g., Falvey, 1974). Additionally, it is possible that the base of the crust was inflated by magmatic intrusion (e.g., Mutter et al., 1982). The margin lacks the large potential fields highs typically associated with magmatic underplating or intrusion, and so significant magmatic inflation of the crust is unlikely. The amount and spatial distribution of erosion of the prerift crust beneath the southwestern Australian marginal basins is unknown, and so the amount of crustal thinning by extension given above may be overestimated.

4.4. Subsidence and Sedimentation History

The highest sedimentation rates encountered in the boreholes are in lithostratigraphic unit V at Site U1513 in the western Mentelle Basin, above the eastern flank of the Naturaliste Plateau (Figure 7). This 250 m
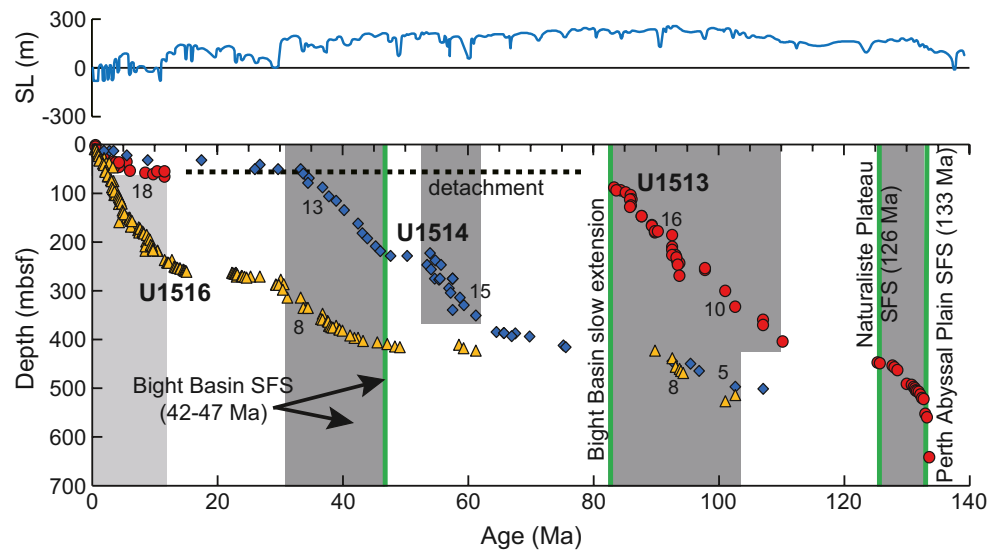
Figure 7. Ages of strata recovered in International Ocean Discovery Program boreholes in the Mentelle Basin as a function of depth below seafloor. Green lines indicate ages of key tectonic events. Shaded areas represent intervals of rapid sedimentation with numbers indicating sedimentation rates (m Myr^{-1}). Site U1515 is not shown due to poor age resolution. Curve at top shows global SL relative to the modern datum (Haq et al., 1987). SFS, onset of seafloor spreading; SL, sea level.

thick unit was deposited between 131 and 121.8 Ma, encompassing the time interval between the Perth Abyssal Plain and Naturaliste Plateau breakup events. Benthic foraminifera indicate water depths increased only slightly during this time, from neritic to upper bathyal (Lee et al., 2020). The amount of tectonic subsidence, S_t, during this period is estimated from the change in the depth to the base of the unit after correcting for sediment and water loading (Steckler & Watts, 1978):

$$S_t = T_u \left(\frac{\rho_m - \rho_s}{\rho_m - \rho_w} \right) + \Delta SF - \Delta SL \left(\frac{\rho_m}{\rho_m - \rho_w} \right) \qquad (2)$$

where T_u is the uncompacted thickness of the unit (273 m: Lee et al., 2020 supplemental data), ΔSL and ΔSF respectively are the changes in eustatic sea level (60 m; Haq, 2014) and seafloor depth that occurred during deposition of the unit, and ρ_m, ρ_s, and ρ_w are the densities of the mantle, sediments, and water, respectively. ΔSF is nominally estimated to be 300 m (the distance between the midpoints of the neritic and upper bathyal depth ranges), with a maximum of 600 m (innermost neritic to lowermost upper bathyal). Using the densities from the previous section, Equation 2 indicates 333–633 m of tectonic subsidence during deposition of unit V, which corresponds to 1,650–3,030 m of crustal thinning (Equation 1). The densities used here are representative of the lithosphere after thermal reequilibration. The proximity of the Kerguelen plume and Perth Abyssal Plain spreading ridge and the relatively high melting temperature estimated for the unit VI basalts suggest hotter conditions at the time of breakup. Assuming an accordingly lower mantle density of 3,100 kg m^{-3} and a higher crust density of 2,900 kg m^{-3} (representing a more mafic crust) results in a similar amount of tectonic subsidence (315–615 m) as the cooler model, but much larger estimates of crustal thinning (3,612–6,762 m). In either case (warm or cool lithosphere), the amount of crustal thinning inferred to have occurred between the Perth Abyssal Plain and Naturaliste Plateau breakup events is less than the total amount of thinning estimated to have occurred on the margin in the previous section (14 km). We conclude that 50%–75% of the thinning at Site U1513 took place prior to the Perth Abyssal Plain breakup event and was most likely coeval with extension in the Perth Basin. We attribute most of this crustal thinning to extensional tectonism, but we note that nonextensional thinning of the lithosphere prior to breakup is also likely to have occurred due to erosion at the top and possibly thermal thinning of the base of the lithosphere. The amounts of these types of thinning are unknown.

Despite 14 km or more of cumulative crustal thinning, the seafloor at Site U1513 remained at neritic depths between the two breakup events on the margin and at upper bathyal depths for 3–5 Myr following the Nat-

uraliste Plateau breakup event (during deposition of the upper part of unit V). The basalts at the top of unit V erupted near the seafloor and underwent no more than about 630 m of tectonic subsidence during this time. The one-dimensional pure shear thinning model of McKenzie (1978) predicts more than 1,200 m of subsidence at Site U1513 using the densities above, the previously estimated extension factor $\beta = 1.9$, and assuming a 125 km thick prerift lithosphere and a mantle potential temperature of 1300°C. We attribute the approximately 570 m deficit in synrift and early postbreakup subsidence on the Naturaliste Plateau to lateral (southward) flow of heat from the Perth Abyssal Plain spreading ridge, which was migrating westward along the northern margins of the Mentelle Basin and Naturaliste Plateau during this time. Alternatively (or in addition), heat from the nearby Kerguelen plume may have kept the margin elevated during rifting. The plume moved southwestward away from the Australian margin after breakup, so its thermal effect on the margin through time would have been similar to that of the Perth Abyssal Plain spreading ridge. Sedimentation rates at Site U1513 were low or zero for approximately 20 Myr following the Naturaliste Plateau breakup event as the margin cooled and subsided to middle bathyal depths (Figure 7).

The postrift depositional hiatus at Site U1513 was followed by a second phase of rapid sedimentation between about 110 Ma and at least 82 Ma (Figure 7). The beginning of the second phase of rapid sedimentation at Site U1513 approximately coincides with the ridge jump at 108 Ma that transferred Gulden Draak and Batavia Knolls from the Indian Plate to the Australian Plate (Gibbons et al., 2012; Whittaker et al., 2016; Williams et al., 2013) (Figure 2e). The second phase of rapid sedimentation may have begun as late as 105 Ma at Sites U1514 and U1516, approximately corresponding with the onset of rifting on the southern margin between Australia and Antarctica (Figure 2f). Sedimentation rates slowed at Sites U1514 and U1516 after about 88 Ma, approximately coinciding with the transition to slow seafloor spreading and/or mantle exhumation on the southern margin by 84 Ma (Figure 2g).

Slow sedimentation continued through the Paleogene, interrupted by periods of relatively rapid sedimentation at Site U1514 between 60 and 55 Ma and at Sites U1514 and U1516 between 47 and 32 Ma (Figure 7). The onset of the latter episode of rapid sedimentation coincides with the transition from slow spreading to normal seafloor spreading on the southern margin between 47 and 42 Ma (Figure 2f). However, we consider it unlikely that either of the Paleogene periods of rapid sedimentation were a direct result of subsidence produced by extension on the southern margin, because the Australian and Antarctic plates presumably became decoupled after slow spreading was established at about 84 Ma. We consider it more likely that changes in the sedimentation rates on the southwestern margin during the Paleogene are a result of changes in carbonate productivity, perhaps influenced by changing ocean circulation patterns as the Southern Ocean opened. Sediment accumulation rates decreased again after about 32 Ma and remained relatively low until 15 Ma at Sites U1513 and U1514 until the present time (increasing slightly after the end of the Miocene Epoch). This Oligocene through middle Miocene interval of low sedimentation rates correlates with an upper Miocene unconformity at DSDP Sites 258 and 264 on the Naturaliste Plateau, which Luyendyk and Davies (1974) attributed to seafloor erosion and nondeposition following establishment of a strong circumpolar current after opening of the Australia-Antarctic seaway during the Oligocene Epoch (J. P. Kennett et al., 1972). The sedimentation rate increased slightly at Sites U1513 and U1514 after about 15 Ma, as has been observed globally (Molnar, 2004), and more dramatically at Site U1516 (Figure 7).

5. Discussion: Implications for Rifting and Magmatism on the Southwest Australian Margin

5.1. Tectonic Evolution and Subsidence

The tectonic, stratigraphic, and magmatic evolution of the southwestern Australian continental margin is summarized schematically in Figure 8. The Late Jurassic through Early Cretaceous rifting that led to opening of the eastern Indian Ocean followed the trend of older north to north-northwest striking rift basins that initially formed during early to middle Permian extension (Veevers, 2006). A period of relative tectonic quiescence and slow thermal subsidence followed, during which time the western Australian margin remained near sea level, as evidenced in the Perth Basin by Early Triassic shallow marine beds grading upward to Early Triassic through Early Jurassic deltaic deposits, coal measures, and red beds (Hall et al., 2013; Norvick, 2004; Veevers, 2006; Yeates et al., 1987) (Figure 8a). Extension was renewed during Middle Jurassic
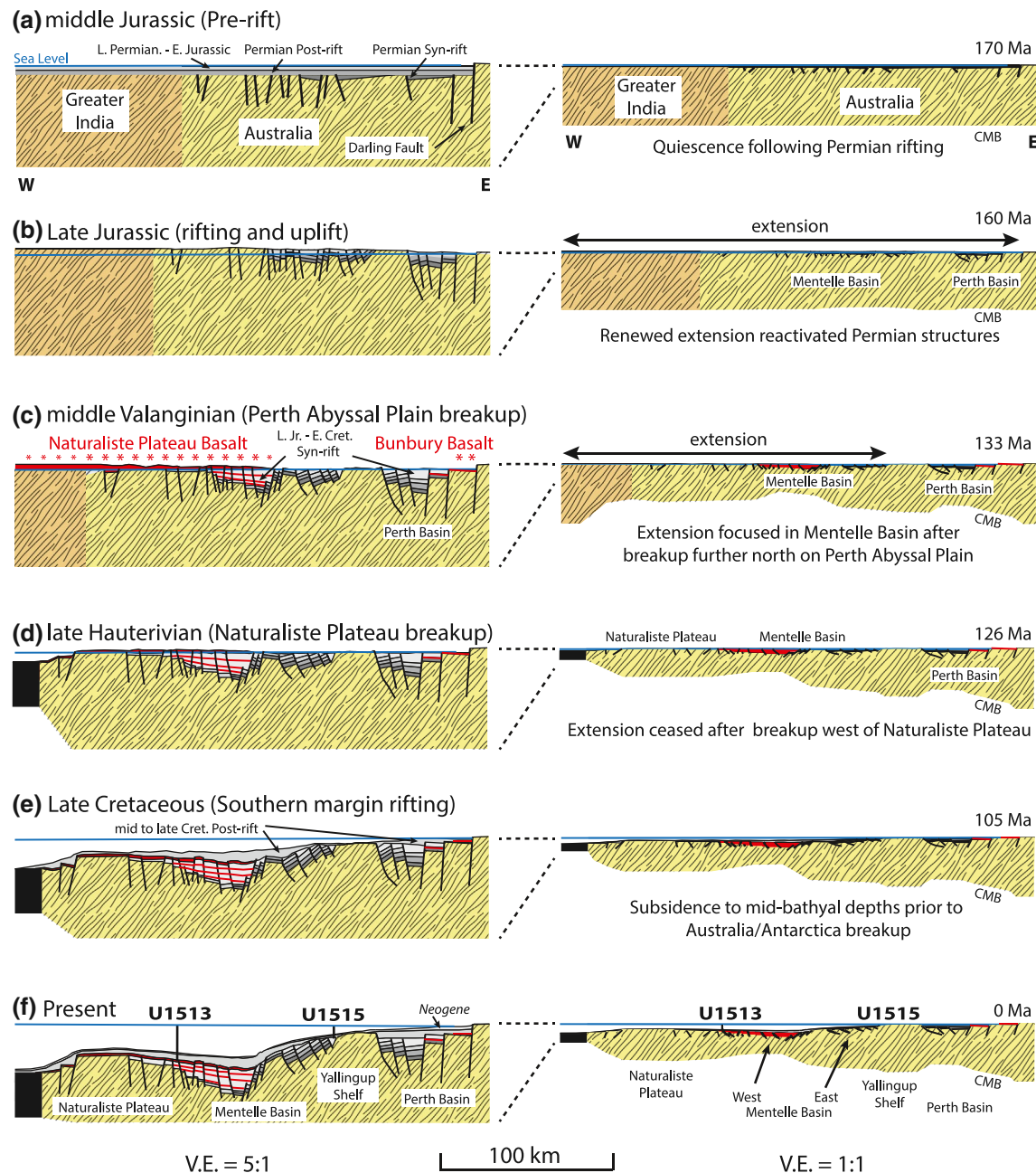
Figure 8. Evolution of the southwest Australian rifted margin. Left column—view of upper crust based on seismic profile S310-05 (Figure 3). Right column—schematic view of entire crust based primarily on gravity studies summarized in text. The profile crosses westward from the eastern edge of the southern Perth Basin across the Yallingup Shelf, Mentelle Basin, and Naturaliste Plateau. Extension direction is northwest (to left and into page) in (c and d), and southward (out of page) in (e and f). (a) Middle Jurassic (prerift). Late Permian through Early Jurassic postrift strata cover synrift strata filling older Middle and Early Permian rift basins. (b) Late Jurassic (early synrift). Onset of rifting between Greater India and Australia, accompanied by formation of fault-bounded rift basins, uplift, and erosion west of the Darling Fault. (c) Late Valanginian (Perth Abyssal Plain breakup). Onset of seafloor spreading on the Perth Abyssal Plain (north of profile), accompanied by basaltic volcanism in the southern Perth Basin and on the Naturaliste Plateau and in the western Mentelle Basin, where extension continues. Flows and sills in rift basin below the unconformity (red) are hypothetical. (d) Early Barremian (Naturaliste Plateau breakup). Greater India and Australia separate and seafloor spreading west of the Naturaliste Plateau begins. Last volcanic eruptions on the Naturaliste Plateau occur immediately after breakup, followed by weathering and redistribution of basaltic material near sea level. (e) Late Cretaceous (immediately prior to breakup between Australia and Antarctica). Most of the margin subsided to midbathyal or greater depths prior to rapid subsidence immediately before the onset of normal seafloor spreading on the southern margin. (f) Rapid postrift subsidence of the central Mentelle Basin followed the onset of seafloor spreading between Australia and Antarctica during the Neogene, producing the modern bathymetry. CMB, crust-mantle boundary.

time, accompanied by faulting and accumulation of Late Jurassic through earliest Cretaceous synrift fluvial and deltaic strata within half-grabens, many of which formed on reactivated Permian faults (Bradshaw et al., 2003; Norvick, 2004). Seismic profiles show abundant faults below the breakup unconformity on the Naturaliste Plateau and in the Perth and Mentelle Basins (Borissova, 2002; Borissova et al., 2010; Hall et al., 2013; Maloney et al., 2011) (Figure 3), indicating that Jurassic through Early Cretaceous extension was accommodated by normal faulting that spanned the breadth of the southwestern Australian margin. Extension was focused most strongly within the central and eastern Mentelle Basin and in the outboard parts of the Perth Basin, where the crust was thinned by factors of $\beta \approx 1.7$–3 and 1.2–1.6, respectively (Olierook et al., 2016, and this study). We interpret the Late Jurassic to earliest Cretaceous fluvio-lacustrine sequence (lithostratigraphic unit IIc) at Site U1515 to be part of the synrift strata that filled one of the several fault-bounded subbasins within the emergent rift. Regional uplift coeval with faulting and filling of the subbasins is indicated by (i) erosional truncation of fault blocks by the breakup unconformity on the flanks of the rift basins (Figure 3) (Borissova, 2002; Borissova et al., 2010; Crostella & Backhouse, 2000; Hall et al., 2013); and (ii) the ages of detrital zircons in the lower part of the synrift strata in the Perth Basin, which indicate dominantly local sources from within the Proterozoic Pinjarra and Albany-Fraser orogens that form the basement beneath the Australian margin (Sircombe & Freeman, 1999). The upper synrift strata are missing in the Perth Basin due to Early Cretaceous erosion at the time of breakup (Bradshaw et al., 2003) (Figure 8b). The Late Jurassic synrift fluvio-lacustrine deposits at Site U1515 transition upward into marine strata (units IIb and IIa), indicating subsidence and marine transgression in the eastern Mentelle Basin beginning in late Valanginian time following breakup and the onset of seafloor spreading on the Perth Abyssal Plain at 132 Ma (Figure 8c).

Emplacement of the Bunbury Basalt in the Perth Basin (137–130 Ma), the basalt flows at Site U1513 (>131 Ma), and the mafic rocks dredged from the margins of the Naturaliste Plateau (132–128 Ma; Direen et al., 2017) were synchronous with seafloor spreading on the Perth Abyssal Plain, but preceded the onset of spreading west of the Naturaliste Plateau. Seismic profiles show many faults in the western Mentelle Basin extend upward into Barremian strata (Borissova, 2002; Borissova et al., 2010), consistent with ongoing extension on this portion of the southwestern Australian margin between the onset of spreading on the Perth Abyssal Plain during the late Valanginian at 133–132 Ma and the onset of spreading west of the Naturaliste Plateau during the early Barremian at 126 Ma (Gibbons et al., 2012; Williams et al., 2013) (Figure 8d). The margin transitioned from volcanically active to inactive between 132 and 126 Ma, with the volcanic sequence deposited atop the breakup unconformity being eroded and re-deposited in the volcanogenic clastic succession on the Naturaliste Plateau (Figure 3c).

Shallow water and/or subaerial emplacement of the basalts at Site U1513, the transition from terrestrial to shallow marine deposition across the stratal equivalent of the unconformity in unit IIb at Site U1515, and the recovery of similar shallow water upper Jurassic strata below the unconformity in the Perth Basin (Crostella & Backhouse, 2000) indicate that the entire southwestern Australian margin was near sea level at the time seafloor spreading began on the Perth Abyssal Plain. Benthic foraminifera and sedimentary features in the epiclastic section overlying the basalt flows at Site U1513 show that the Naturaliste Plateau remained at or near neritic depths following the Perth Abyssal Plain breakup event at 133–132 Ma, and at upper bathyal depths for at least 3 Myr following the Naturaliste Plateau breakup event at 126 Ma. The margin underwent no more than about 630 m of tectonic subsidence between the two breakup events, in spite of ongoing extension. The lack of greater amounts of subsidence during the final stages of rifting and immediately afterward can be attributed to the proximity of either (i) the Perth Abyssal Plain spreading ridge, which was migrating westward along the northern edges of the Mentelle Basin and Naturaliste Plateau between 132 Ma and 124 Ma, or (ii) the Kerguelen plume, which was moving southwestward away from the margin during this time. The approximately 1400°C mantle potential temperature indicated by petrogenetic modeling of the basalt compositions at Site U1513 supports the presence of a warm buoyant plume head beneath the rift at the time of breakup.

The onset of a depositional hiatus and the end of deposition of the volcanogenic clastic strata (unit V) on the Naturaliste Plateau occurred at chron M0r time (Lee et al., 2020), coinciding with a westward jump of the Perth Basin spreading ridge away from the Australian margin (Gibbons et al., 2012). We infer that thermal subsidence of the Naturaliste Plateau began at this time, as the marine claystones of unit IV at Site U1513

indicate that the eastern Naturaliste Plateau had reached at least middle bathyal depths by early Albian time (110 Ma) (Figure 8e). We attribute the reduction in sedimentation rate after deposition of unit V to the increased depth of the plateau and the corresponding reduction in the supply of clastic sediments weathered from the subsiding volcanic terranes. Sediment from potential distal sources in Greater India and Australia would have been prevented from reaching the Naturaliste Plateau by the newly opened seaway to the west and by the subsiding Mentelle Basin to the east. The water depth in the central Mentelle Basin (Sites U1514 and U1516) is loosely constrained to have been within the broad bathyal depth range in early Albian time.

Following the depositional hiatus at Site U1513, a period of relatively rapid sedimentation occurred on the Naturaliste Plateau (Site U1513) and in the central Mentelle Basin (U1514 and U1516) beginning between 110 and 100 Ma and lasting to at least 82 Ma (Figure 7). The beginning of this period of rapid sedimentation was coincident with a westward jump of the Indian Ocean spreading ridge at 108 Ma and with the onset of rifting on the southern Australian margin. The high sedimentation rates during this period may reflect ongoing thermal subsidence on the margin after breakup between Australia and Greater India, possibly with increased sediment input from the southern rift, or it may reflect subsidence related to extension on the southern margin. The latter possibility is supported by the modest decrease in sedimentation rates after about 88 Ma at Sites U1515 and U1516, which may indicate decreased coupling between the Australian and Antarctic plates as slow spreading developed on the southern margin. Another interval of relatively rapid sedimentation in the central Mentelle Basin (Sites U1514 and U1516) began at about 47 Ma, when normal seafloor spreading was established and final separation occurred between Australia and Antarctica (this was preceded at Site U1514 by a short interval of rapid sedimentation between 60 and 55 Ma). The periods of rapid sedimentation beginning at 100, 60, and 47 Ma correlate with tectonic events on the southern margin, but we note that the post-Aptian strata are carbonate rich and so thickness changes are not necessarily indicative of subsidence. The post-Aptian changes in sedimentation rate may be due to increased productivity in the water column that resulted from changes in ocean circulation patterns that occurred as the new seaway opened between Australian and Antarctica. Except for accumulation of about 250 m of carbonates in the southern part of the central Mentelle Basin (Site U1516), the margin has experienced little deposition since late Oligocene time as it subsided to its modern lower bathyal to abyssal (>2000 m) water depths (Figure 8f).

5.2. Petrogenesis and Distribution of Synrift Basalts and Relation to the Kerguelen Plume

Petrogenetic modeling suggests that the most primitive basalts recovered at IODP Site U1513 were generated from approximately 25% melting of a lherzolite source at 1.5 GPa (approximately 50 km depth) and a mantle potential temperature of about 1400°C (with estimated primary magma temperatures ranging from 1369°C to 1413°C). This temperature is high compared to the global average, which typically ranges from 1250°C to 1350°C (Gudfinnsson & Presnall, 2005; Kimura and Kawabata, 2015; McKenzie & Bickle, 1988; McKenzie et al., 2005; Presnall et al., 2002), although global average potential temperatures as high as 1420°C have been suggested (Herzberg et al., 2007; Putirka, 2005). The relatively high potential temperature seems indicative of the presence of an active or recently active plume at the time of breakup. The estimated mantle temperature is ≥ 100°C lower than expected for the axis of a plume, but within the expected range for a broad plume head (Campbell & Griffiths, 1990; R. S. White and McKenzie, 1995). The melting conditions are thus consistent with either a large diameter Kerguelen plume head beneath the northeastern Indian Ocean during the Early Cretaceous Period (Direen et al., 2017; Olierook et al., 2016, 2017; Storey et al., 1989), or with multiple limbs from a fragmented or dismembered plume (Coffin et al., 2002).

The Bunbury Basalt and the basalt flows encountered in the western Mentelle Basin at IODP Site U1513 represent late synrift and early postrift magmatism that, although geographically widespread, has a relatively small net thickness for plume-related volcanism. The moderately high mantle potential temperature inferred from the Naturaliste Plateau basalts (1400°C) suggests a larger thickness of melt should have been produced during earlier stages of rifting, particularly in the highly extended central Mentelle Basin (where β > 3) (e.g., McKenzie & Bickle, 1988). Possible evidence of such earlier synrift magmatism are high-amplitude seismic reflectors imaged within the thick undrilled stratified interval below the lowermost (Valanginian) breakup unconformity in the central and western Mentelle Basin (Figure 9). These high-am-
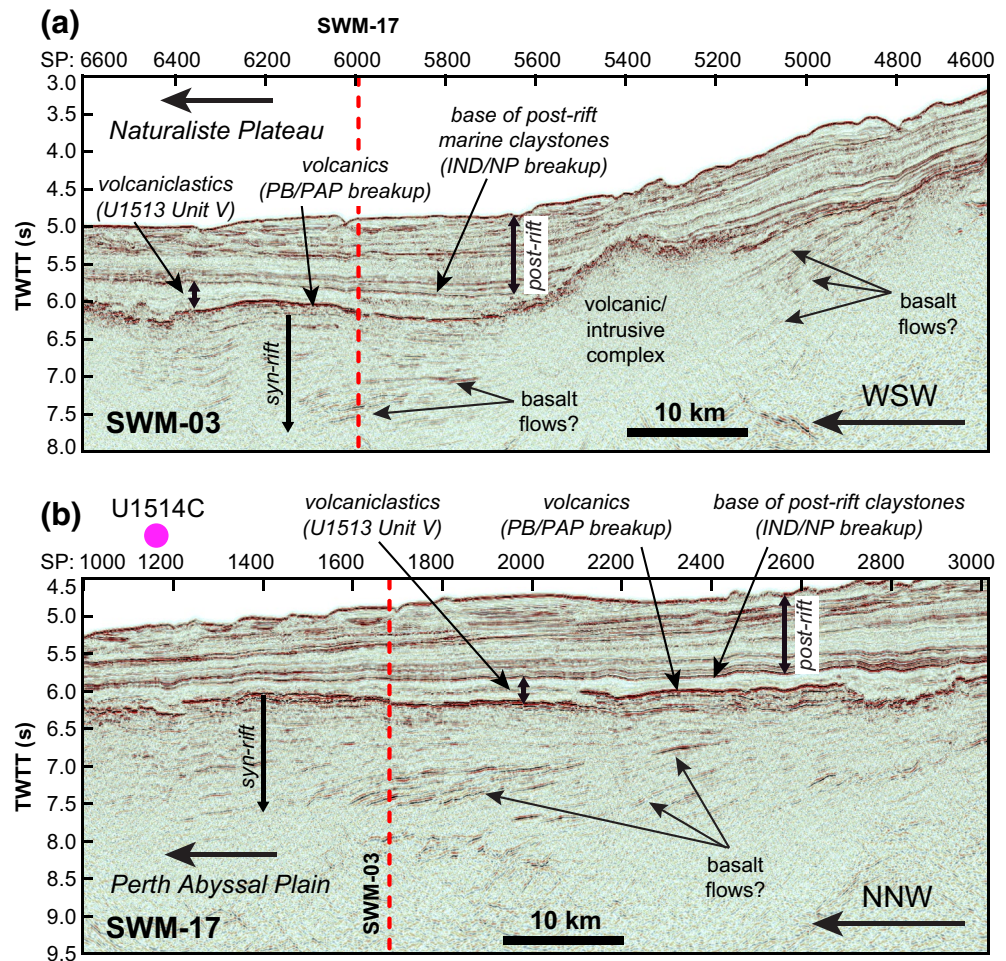
Figure 9. Seismic reflection profiles showing high amplitude reflectors interpreted to be basalt flows. (a) Profile S310-17 trending WSW across the Mentelle Basin, showing probable volcanic/intrusive complex and associated flows that lies along strike of the Perth Basin/Perth Abyssal Plain ocean-continent transition further north. (b) Profile S310-03 trending NNW, showing reflectors that dip toward the ocean-continent boundary at the south edge of the Perth Abyssal Plain. Vertical dashed red line marks intersection of the two profiles. Profile locations shown in Figure 1. Seismic profiles available from Geoscience Australia National Offshore Petroleum Information Management System (https://nopims.dmp.wa.gov.au/nopims).

plitude reflectors could be produced by basalt flows interbedded within the Late Cretaceous synrift strata that has been previously interpreted to fill the fault bounded rift basins below the Valanginian breakup unconformity (Borissova et al., 2010; Maloney et al., 2011). Seismic velocities in this interval average about 6 km s^{-1} (Maloney et al., 2011), which is high compared to most siliclastic rocks, which typically range from about 2.5 to 5.0 km s^{-1} (Castagna et al, 1985). The seismic velocity of basalt typically ranges from about 5.2 to 6.5 km s^{-1} (Christensen & Stanley, 2003). Assuming a basalt velocity of 6.5 km s^{-1} (appropriate for low porosity flows or sills), volume averaging of the velocities suggests 67%–88% of the material filling the rift basins below the Valanginian unconformity in the central and western Mentelle Basin could be basaltic. Substantially larger volumes of basalt (up to 100%) may be implied if the basalt velocity is lower than 6.5 km s^{-1}, although this seems unlikely given the similarity of the deep reflections in the western Mentelle Basin with those imaged within the Permian and Jurassic synrift sedimentary strata further east on the margin in the Perth Basin (e.g., Borissova et al., 2010).

Alternatively, little basalt (potentially none) below the Valanginian breakup unconformity may be implied if the high velocity in the synrift clastic sediments is due to hydrothermal cementation, as is observed in the volcaniclastic sediments in unit V and in the interbedded flows of unit VI at IODP Site U1513. In such a case,

the Bunbury Basalt and the basalts of the western Mentelle Basin and Naturaliste Plateau may represent minor late-stage magmatism that occurred immediately prior to breakup on an otherwise amagmatic segment of the western Australia rifted margin. This is consistent with the model of Olierook et al. (2016), who suggested that the Bunbury Basalt originated from decompression melting of fertile domains in the upper mantle that were themselves products of older metasomatic episodes. However, although melting of fertile components may be a sufficient explanation for the Bunbury Basalt, the relatively high mantle temperature inferred from the Site U1513 basalts indicates some influence from a hot plume. This favors a hybrid interpretation, in which the Bunbury Basalt in the moderately extended southern Perth Basin is a result of melting of fertile domains within a metasomatized lithospheric mantle, whereas the basalts of the more highly extended central and western Mentelle Basin may be products of decompression melting of a warm sublithospheric mantle plume head or plume limb.

6. Summary

IODP Expedition 369 drilled four sites on the southwestern Australian continental margin. At Site U1513, located in the western Mentelle Basin above the eastern flank of the Naturaliste Plateau, drilling penetrated into Early Cretaceous interbedded basalt flows and volcaniclastic layers that lie immediately above the seismically imaged breakup unconformity. Sites U1514 and U1516, located in the central Mentelle Basin, penetrated into an Early Cretaceous (Albian) postrift marine claystone unit. Drilling at Site U1515, near the eastern edge of the Mentelle Basin, penetrated through the postrift sequence and into late synrift lacustrine deposits. Drilling shows the seismically imaged breakup unconformity on the Naturaliste Plateau and in the western Mentelle Basin to be equivalent to the late Valanginian breakup unconformity that is present in the Perth Basin, which extends for 1,000 km along the western Australian margin beneath the continental shelf. The late Valanginian unconformity marks the onset of seafloor spreading on the Perth Abyssal Plain, which is inferred to have begun between chrons M11r and M11n (133–132 Ma). In the western Mentelle Basin/Naturaliste Plateau (Site U1513), the Valanginian unconformity is overlain by basalt flows and interlayered volcaniclastic beds that were sampled in situ for the first time during IODP Expedition 369. Petrogenetic modeling indicates these basalts formed by approximately 25% melting of a lherzolite mantle source at 1.5 GPa and with a mantle potential temperature of 1400°C. This moderately high mantle potential temperature is most easily accounted for by the presence of a large Kerguelen plume head beneath the eastern Indian Ocean at the time of breakup, although the trace element geochemistry and melting trends also suggest involvement of a mid-ocean ridge component. The magnetostratigraphy of the overlying strata show that the basalt flows at Site U1513 predate the end of chron M10Nn.1n (131 Ma). The breakup unconformity below the basalts is interpreted to have formed when seafloor spreading began on the Perth Abyssal Plain, no earlier than chron M11r (133 Ma). This implies that the flows encountered at Site U1513 were emplaced between 132 and 133 Ma, immediately after (or synchronous with) the onset of seafloor spreading on the Perth Abyssal Plain and contemporaneous with the Bunbury Basalt found in the southern Perth Basin. In the eastern Mentelle Basin at Site U1515, breakup on the Perth Abyssal Plain manifests as a rapid conformable upward transition from Late Jurassic to earliest Cretaceous synrift fluvio-lacustrine strata deposited in a fault bounded rift basin into transgressive marine strata deposited after breakup.

At Site U1513, the basalt flows are overlain by a 235 m thick epiclastic sequence deposited mostly at shelf depths that contains abundant weathered volcanic materials, presumably sourced from local volcanic edifices. These strata demonstrate that the eastern Naturaliste Plateau remained at shallow depths for 3–5 Myr following breakup on the Perth Abyssal Plain. The uppermost part of the volcanogenic epiclastic strata contains marine silty claystone that was deposited in upper bathyal depths. This is interpreted to be the lower part of the postrift sequence, deposited after the second breakup event on the margin at 126 Ma that marked final separation of Greater India from Australia and the onset of seafloor spreading to the west of the Naturaliste Plateau.

Pillow structures and oxidation show that the basalt flows on the eastern Naturaliste Plateau and in the western Mentelle Basin (Site U1513) were erupted subaerially or in shallow water, indicating that the southwestern Australian margin was near sea level when seafloor spreading began on the Perth Abyssal Plain. The Naturaliste Plateau remained at shelf depths during the 6–9 Myr period between breakup on the Perth

Abyssal Plain to the north (132–133 Ma) and final breakup with Greater India to the west (124–126 Ma), and subsided to only upper bathyal depths during the 3–5 Myr period after the final breakup event. The lack of greater subsidence during this late synrift and early postrift period is attributed to heat from the nearby Perth Abyssal Plain spreading ridge, which migrated westward along the northern margins of the Naturaliste Plateau and Mentelle Basin between 132 and 124 Ma, and to proximity of the Kerguelen plume. A depositional hiatus or period of slow sedimentation occurred at Site U1513 on the Naturaliste Plateau between 121 and 110 Ma as the plateau and central Mentelle Basin (Sites U1514 and U1516) subsided to middle bathyal depths. Periods of rapid deposition occurred in the Late Cretaceous (100 Ma) and again in Paleogene time (47 Ma), coinciding respectively with the onset of rifting between Australia and Antarctica and with breakup and establishment of normal seafloor spreading on the southern margin. High sedimentation rates in the Paleogene are likely due to increased carbonate productivity on the margin that resulted from establishment of a new ocean circulation pattern following separation of Antarctica from Australia.

Data Availability Statement

Downhole geological, geophysical, and geochemical datasets used in this research are accessible through the following International Ocean Discover Program publications and their supplemental information files: Hobbs et al. (2019) and Huber et al. (2019a), available online at http://publications.iodp.org/proceedings/369/369title.html. Seismic reflection profiles shown in this study are available from Geoscience Australia National Offshore Petroleum Information Management System (https://nopims.dmp.wa.gov.au/nopims). X-ray fluorescence spectrometry data for volcanic and volcaniclastic samples recovered at IODP Site U1513 are available at the PANGEA website (doi:https://doi.pangaea.de/10.1594/PANGAEA.924535).

References

Aguirre-Urreta, B., Martinez, M., Schmitz, M., Lescano, M., Omarini, J., Tunik, M., et al. (2019). Interhemispheric radio-astrochronological calibration of the time scales from the Andean and the Tethyan areas in the Valanginian–Hauterivian (Early Cretaceous). *Gondwana Research*, *70*, 104–132. https://doi.org/10.1016/j.gr.2019.01.006

Ali, J. R., & Aitchison, J. C. (2014). Greater India's northern margin prior to its collision with Asia. *Basin Research*, *26*, 73–84. https://doi.org/10.1111/bre.12040

Ariskin, A. A. (1999). Phase equilibria modeling in igneous petrology: Use of COMAGMAT model for simulating fractionation of ferro-basaltic magmas and the genesis of high-alumina basalt. *Journal of Volcanology and Geothermal Research*, *90*, 115–162. https://doi.org/10.1016/S0377-0273(99)00022-0

Baksi, A. K. (1995). Petrogenesis and timing of volcanism in the Rajmahal flood basalt province, northeastern India. *Chemical Geology*, *121*, 73–90. https://doi.org/10.1016/0009-2541(94)00124-Q

Baksi, A. K., Barman, T. R., Paul, D., & Farrar, E. (1987). Widespread Early Cretaceous flood basalt volcanism in eastern India: Geochemical data from the Rajmahal-Bengal-Sylhet traps. *Chemical Geology*, *63*, 133–141. https://doi.org/10.1016/0009-2541(87)90080-5

Ball, P., Eagles, G., Ebinger, C., McClay, K., & Totterdell, J. M. (2013). The spatial and temporal evolution of strain during the separation of Australia and Antarctica. *Geochemistry, Geophysics, Geosystems*, *14*, 2771–2799. https://doi.org/10.1002/ggge.20160

Besse, J., & Courtillot, V. (1988). Paleogeographic maps of the continents bordering the Indian ocean since the early Jurassic. *Journal of Geophysical Research*, *93*, 11791–11808. https://doi.org/10.1029/JB093iB10p11791

Bodin, S., Godet, A., Föllmi, K. B., Vermeulen, J., Arnaud, H., Strasser, A., et al. (2006). The late Hauterivian Faraoni oceanic anoxic event in the western Tethys: Evidence from phosphorus burial rates. *Palaeogeography, Palaeoclimatology, Palaeoecology*, *235*, 245–264. https://doi.org/10.1016/j.palaeo.2005.09.030

Borissova, I. (2002). *Geological framework of the Naturaliste Plateau, Geoscience Australia Record 2002/20* (p. 44). Canberra, Australia: Geoscience Australia.

Borissova, I., Bradshaw, B. E., Nicholson, C. J., Struckmeyer, H. I. M., & Payne, D. (2010). New exploration opportunities on the southwest Australian margin—Deep-water frontier Mentelle Basin. *The APPEA Journal*, *50*, 47–58. https://doi.org/10.1071/AJ09004

Bradshaw, B. E., Rollet, N., Totterdell, J. M., & Borissova, I. (2003). *A revised structural framework for frontier basins on the southern and southwestern Australian continental margin, Geoscience Australia Record 2003/03* (p. 43). Canberra, Australia: Geoscience Australia.

Campbell, I. H., & Griffiths, R. W. (1990). Implications of mantle plume structure for the evolution of flood basalts. *Earth and Planetary Science Letters*, *99*, 79–93. https://doi.org/10.1016/0012-821X(90)90072-6

Cande, S. C., & Mutter, J. C. (1982). A revised identification of the oldest sea-floor spreading anomalies between Australia and Antarctica. *Earth and Planetary Science Letters*, *58*, 151–160. https://doi.org/10.1016/0012-821X(82)90190-X

Castagna, J. P., Batzle, M. L., & Eastwood, R. L. (1985). Relationships between compressional-wave and shear-wave velocities in clastic silicate rocks. *Geophysics*, *50*(4), 571–581. https://doi.org/10.1190/1.1441933

Christensen, N. L., & Stanley, D. (2003). Seismic velocities and densities of rocks. In W. Lee, H. Kanamori, P. Jennings, & C. Kisslinger (Eds.), *International handbook of earthquake and engineering seismology* (Vol. 81B, pp. 1587–1594). Amsterdam, The Netherlands: Elsevier. https://doi.org/10.1016/S0074-6142(03)80278-4

Coffin, M. F., Pringle, M. S., Duncan, R. A., Gladzenko, T. P., Storey, M., Müller, R. D., & Gahagan, L. A. (2002). Kerguelen hotspot magma output since 130 Ma. *Journal of Petrology*, *43*, 1121–1139. https://doi.org/10.1093/petrology/43.7.1121

Coleman, P. J., Michael, P. J., & Mutter, J. C. (1982). The origin of the Naturaliste Plateau, SE Indian Ocean: Implications from dredged basalts. *Journal of the Geological Society of Australia*, *29*, 457–468. https://doi.org/10.1080/00167618208729228

Colwell, J. B., Symonds, P. A., & Crawford, A. J. (1994). The nature of the Wallaby (Cuvier) Plateau and other igneous provinces of the west Australian margin. *Journal of Australian Geology and Geophysics*, *15*, 137–156.

Crostella, A., & Backhouse, J. (2000). *Geology and petroleum exploration of the central and southern Perth Basin, western Australia, report 57* (p. 85). Perth, Australia: Geological Survey of Western Australia.

Davies, T. A., Luyendyk, B. P., Rodolfo, K. S., Kempe, D. R. C., McKelvey, B. C., Leidy, R. D., et al. (1974). *Initial Reports of the Deep Sea Drilling Project* (Vol. 26, pp. 359–414, Site 258). Washington, DC: U.S. Government Printing Office. https://doi.org/10.2973/dsdp.proc.26.111.1974

Dentith, M. C., Dent, V. F., & Drummond, B. J. (2000). Deep crustal structure in the southwestern Yilgarn Craton, Western Australia. *Tectonophysics*, *325*, 227–255. https://doi.org/10.1016/S0040-1951(00)00119-0

Direen, N. G., Borissova, I., Stagg, H. M. J., Colwell, J. B., & Symonds, P. A. (2007). Nature of the ocean-continent transition along the southern Australian continental margin: a comparison of the Naturaliste Plateau, SW Australia, and the central Great Australian Bight sectors. In G. D. Karner, G. Manatschal, & L. M. Punheiro (Eds.), *Imaging, mapping, and modeling continental lithosphere extension and breakup* (pp. 239–263). London, UK: Geological Society. https://doi.org/10.1144/SP282.12

Direen, N. G., Cohen, B. E., Maas, R., Frey, F. A., Whittaker, J. M., Coffin, M. F., et al. (2017). Naturaliste Plateau: Constraints on the timing and evolution of the Kerguelen Large Igneous province and its role in Gondwana breakup. *Australian Journal of Earth Sciences*, *64*(7), 851–869. https://doi.org/10.1080/08120099.2017.1367326

Direen, N. G., Stagg, H. M. J., Symonds, P. A., & Colwell, J. B. (2008). Architecture of volcanic rifted margins: New insights from the Exmouth-Gascoyne margin, Western Australia. *Australian Journal of Earth Sciences*, *55*, 341–363. https://doi.org/10.1080/08120090701769472

Direen, N. G., Stagg, H. M. J., Symonds, P. A., & Colwell, J. B. (2011). Dominant symmetry of a conjugate southern Australian and East Antarctic magma-poor rifted margin segment. *Geochemistry, Geophysics, Geosystems*, *12*, Q02006. https://doi.org/10.1029/2010GC003306

Dosso, L., Bougault, H., Beuzart, P., Calvez, J.-Y., & Joron, J.-L. (1988). The geochemical structure of the South-East Indian Ridge. *Earth and Planetary Science Letters*, *88*, 47–59. https://doi.org/10.1016/0012-821X(88)90045-3

Doucet, S., Scoates, J. S., Weis, D., & Giret, A. (2005). Constraining the components of the Kerguelen mantle plume: A Hf-Pb-Sr-Nd isotopic study of picrites and high-MgO basalts from the Kerguelen Archipelago. *Geochemistry, Geophysics, Geosystems*, *6*(4), Q04007. https://doi.org/10.1029/2004GC000806

Duncan, R. A. (2002). A time frame for construction of the Kerguelen Plateau and Broken Ridge. *Journal of Petrology*, *43*, 1109–1119. https://doi.org/10.1093/petrology/43.7.1109

Falvey, D. A. (1974). The development of continental margins in plate tectonic theory. *The APPEA Journal*, *14*(1), 95–106. https://doi.org/10.1071/AJ73012

Fisher, R. V. (1961). Proposed classification of volcaniclastic sediments and rocks. *Geological Society of America Bulletin*, *72*, 1409–1414. https://doi.org/10.1130/0016-7606(1961)72[1409:PCOVSA]2.0.CO;2

Ford, A. B. (1975). Volcanic rocks of Naturaliste Plateau, eastern Indian Ocean, Site 264, DSDP leg 28. In *Initial Reports of the Deep Sea Drilling Project* (Vol. 28, pp. 821–833). Washington, DC: U.S. Government Printing Office.

Frau, C., Bulot, L. G., Delanoy, G., Moreno-Bedmar, J. A., Masse, J.-P., Tendil, A., & Lanteaume, C. (2018). The Aptian GSSP candidate at Gorgo a Cerbara (Central Italy): an alternative interpretation of the bio-, litho- and chemostratigraphic markers. *Newsletters on Stratigraphy*, *51*, 311–326. https://doi.org/10.1127/nos/2017/0422

Frey, F. A., Coffin, M. F., Wallace, P. J., Weis, D., Zhao, X., Wise, S. W., Jr., et al. (2000). Origin and evolution of a submarine large igneous province: The Kerguelen Plateau and Broken Ridge, southern Indian Ocean. *Earth and Planetary Science Letters*, *176*, 73–89. https://doi.org/10.1016/S0012-821X(99)00315-5

Frey, F. A., McNaughton, N. J., Nelson, D. R., & Duncan, R. A. (1996). Petrogenesis of the Bunbury Basalt, Western Australia: Interaction between the Kerguelen plume and Gondwana lithosphere? *Earth and Planetary Science Letters*, *144*, 163–183. https://doi.org/10.1016/0012-821X(96)00150-1

Fullerton, L. G., Sager, W. W., & Handschumacher, D. W. (1989). Late Jurassic-Early Cretaceous evolution of the eastern Indian Ocean adjacent to northwest Australia. *Journal of Geophysical Research*, *94*, 2937–2953. https://doi.org/10.1029/JB094iB03p02937

Gaina, C., Müller, R. D., Brown, B., Ishihara, T., & Ivanov, S. (2007). Breakup and early seafloor spreading between India and Antarctica. *Geophysical Journal International*, *170*, 151–169. https://doi.org/10.1111/j.1365-246X.2007.03450.x

Gee, J. S., & Kent, D. V. (2007). Source of oceanic magnetic anomalies and the Geomagnetic Time Scale. *Treatise on Geophysics*, *5*, 455–507. https://doi.org/10.1016/B978-044452748-6.00097-3

Gibbons, A. D., Barckhausen, U., van den Bogaard, P., Hoernle, K., Werner, R., Whittaker, J. M., & Müller, R. D. (2012). Constraining the Jurassic extent of Greater India: Tectonic evolution of the West Australian margin. *Geochemistry, Geophysics, Geosystems*, *13*, Q05W13. https://doi.org/10.1029/2011GC003919

Gibbons, A. D., Whittaker, J. M., & Müller, R. D. (2013). The breakup of East Gondwana: Assimilating constraints from Cretaceous ocean basins around India into a best-fit tectonic model. *Journal of Geophysical Research: Solid Earth*, *118*, 808–822. https://doi.org/10.1002/jgrb.50079

Goncharov, A., & Nelson, G. (2012). From two way time to depth and pressure for interpretation of seismic velocities offshore: Methodology and examples from the Wallaby Plateau on the West Australian margin. *Tectonophysics*, *572–573*, 26–37. https://doi.org/10.1016/j.tecto.2012.06.037

Gudfinnsson, G. H., & Presnall, D. C. (2005). Continuous gradations among primary carbonatitic, kimberlitic, melilititic, basaltic, picritic, and komatiitic melts in equilibrium with garnet lherzolite at 3–8GPa. *Journal of Petrology*, *46*, 1645–1659. https://doi.org/10.1093/petrology/egi029

Hall, L. S., Gibbons, A. D., Bernardel, G., Whittaker, J., Nicholson, C., Rollet, N., & Müller, R. D. (2013), Structural architecture of Australia's southwest continental margin and implications for Early Cretaceous basin evolution. In S. J. Moss & M. Keep (Eds.), *West Australian Basins Symposium* (pp. 2–20). Perth, Australia: Petroleum Exploration Society of Australia.

Halpin, J. A., Crawford, A. J., Direen, N. G., Coffin, M. F., Forbes, C. J., & Borissova, I. (2008). Naturaliste Plateau, offshore Western Australia: A submarine window into Gondwana assembly and breakup. *Geology*, *36*, 807–810. https://doi.org/10.1130/G25059A.1

Halpin, J. A., Daczko, N. R., Direen, N. G., Mulder, R. C., & Ishihara, T. (2020). Provenance of rifted continental crust at the nexus of East Gondwana breakup. *Lithos*, *354–355*, 105363. https://doi.org/10.1016/j.lithos.2019.105363

Haq, B. U. (2014). Cretaceous eustacy revisited. *Global and Planetary Change*, *113*, 44–58. https://doi.org/10.1016/j.gloplacha.2013.12.007

Haq, B. U., Hardenbol, J., & Vail, P. R. (1987). Chronology of fluctuating sea levels since the Triassic. *Science*, *235*, 1156–1167. https://doi.org/10.1126/science.235.4793.1156

Harris, L. B. (1994). Structural and tectonic synthesis for the Perth Basin, western Australia. *Journal of Petroleum Geology*, *17*, 129–156. https://doi.org/10.1111/j.1747-5457.1994.tb00123.x

Harrowfield, M., Holdgate, G. R., Wilson, C. J. L., & McLoughlin, S. (2005). Tectonic significance of the Lambert graben, East Antarctica: Reconstructing the Gondwanan rift. *Geology*, *33*, 197–200. https://doi.org/10.1130/G21081.1

Heine, C., & Müller, R. (2005). Late Jurassic rifting along the Australian North West Shelf: margin geometry and spreading ridge configuration. *Australian Journal of Earth Sciences*, *52*, 27–39. https://doi.org/10.1080/08120090500100077

Herzberg, C., Asimow, P. D., Arndt, N., Niu, Y., Lesher, C. M., Fitton, J. G., et al. (2007). Temperatures in ambient mantle and plumes: Constraints from basalts, picrites, and komatiites. *Geochemistry, Geophysics, Geosystems*, *8*, Q02006. https://doi.org/10.1029/2006GC001390

Herzberg, C., & Asimow, P. D. (2008). Petrology of some oceanic island basalts: PRIMELT2.XLS software for primary magma calculation. *Geochemistry, Geophysics, Geosystems*, *9*, Q09001. https://doi.org/10.1029/2008GC002057

Hobbs, R. W., Huber, B. T., Bogus, K. A., Batenburg, S. J., Brumsack, H.-J., do Monte Guerra, R., et al. (2019). *Expedition 369: Australia cretaceous climate and tectonics* (Vol. 369). Proceedings of the International Ocean Discovery Program, International Ocean Discovery Program, College Station, TX.

Huber, B. T., Hobbs, R. W., Bogus, K. A., Batenburg, S. J., Brumsack, H.-J., do Monte Guerra, R., et al. (2018). *Expedition 369 preliminary report: Australia Cretaceous climate and tectonics* (p. 39). College Station, TX: International Ocean Discovery Program.

Huber, B. T., Hobbs, R. W., Bogus, K. A., Batenburg, S. J., Brumsack, H.-J., do Monte Guerra, R., et al. (2019a). *Australia Cretaceous climate and tectonics* (Vol. 369, Site U1513). Proceedings of the International Ocean Discovery Program, International Ocean Discovery Program, College Station, TX. https://doi.org/10.14379/iodp.proc.369.104.2019

Huber, B. T., Hobbs, R. W., Bogus, K. A., Batenburg, S. J., Brumsack, H.-J., do Monte Guerra, R., et al. (2019b). *Australia Cretaceous climate and tectonics* (Vol. 369, Site U1515). Proceedings of the International Ocean Discovery Program, International Ocean Discovery Program, College Station, TX. https://doi.org/10.14379/iodp.proc.369.106.2019

Ingle, S., Scoates, J., Weis, D., Brügmann, G., & Kent, R. (2004). Origin of Cretaceous continental tholeiites in southwestern Australia and eastern India: Insights from Hf and Os isotopes. *Chemical Geology*, *209*, 83–106. https://doi.org/10.1016/j.chemgeo.2004.04.023

Ingle, S., Weis, D., Scoates, J. S., & Frey, F. A. (2002). Relationship between the early Kerguelen plume and continental flood basalts of the paleo-Eastern Gondwanan margins. *Earth and Planetary Science Letters*, *197*, 35–50. https://doi.org/10.1016/S0012-821X(02)00473-9

Johnston, S., Hackney, R., & Nicholson, C. (2010). Distribution of igneous facies and potential-field modelling of the Mentelle Basin, southwestern margin, Australia. *Australian Society of Exploration Geophysicists Extended Abstracts*, *2010*, 1–4. https://doi.org/10.1081/22020586.2010.12041965

Kennett, J. P., Burns, R. E., Andrews, J. E., Churkin, M., Davies, T. A., Dumitrica, P., et al. (1972). Australian-Antarctic continental drift, paleocirculation changes and Oligocene deep-sea erosion. *Nature Physical Science*, *239*, 51–55.

Kennett, B. L. N., Salmon, M., & Saygin, E. (2011). AusMoho Working GroupAusMoho: The variation of Moho depth in Australia. *Geophysical Journal International*, *187*, 946–958. https://doi.org/10.1111/j.1365-246X.2011.05194.x

Kent, R. (1991). Lithospheric uplift in eastern Gondwana: evidence for a long-lived mantle plume system. *Geology*, *19*, 19–23. https://doi.org/10.1130/0091-7613(1991)019<0019:LUIEGE>2.3.CO;2

Kent, R. W., Pringle, M. S., Müller, R. D., Saunders, A. D., & Ghose, N. C. (2002). 40Ar/39Ar geochronology of the Rajmahal basalts, India, and their relationship to the Kerguelen Plateau. *Journal of Petrology*, *43*, 1141–1153. https://doi.org/10.1093/petrology/43.7.1141

Kimura, J.-I., & Ariskin, A. A. (2014). Calculation of water-bearing primary basalt and estimation of source mantle conditions beneath arcs: PRIMACALC2 model for WINDOWS. *Geochemistry, Geophysics, Geosystems*, *15*, 1494–1514. https://doi.org/10.1002/2014GC005329

Kimura, J.-I., & Kawabata, H. (2015). Ocean Basalt Simulator version 1 (OBS1): Trace element mass balance in adiabatic melting of a pyroxenite-bearing peridotite. *Geochemistry, Geophysics, Geosystems*, *16*, 267–300. https://doi.org/10.1002/2014GC005606

Kurnosov, V., Zolotarev, B., Artamonov, A., Garanina, S., Petrova, V., Eroshchev-Shak, V., & Sokolova, A. (2003). *Data report: Alteration of basalts from the Kerguelen Plateau* (Vol. 183, pp. 1–40). Proceedings of the Ocean Drilling Program, Scientific Results, Ocean Drilling Program, College Station, TX.

Le Bas, M. J., Le Maitre, R., Streckeisen, A., & Zanettin, B. (1986). A chemical classification of volcanic rocks based on the total alkali-silica diagram. *Journal of Petrology*, *27*, 745–750. https://doi.org/10.1093/petrology/27.3.745

Lee, E. Y., Novotny, J., & Wagreich, M. (2019). *Subsidence analysis and visualization for sedimentary basin analysis and modelling*. New York, NY: Springer. https://doi.org/10.1007/978-3-319-76424-5

Lee, E. Y., Wolfgring, E., Tejada, M. L. G., Harry, D. L., Wainman, C. C., Chun, S. S., et al. (2020). Early cretaceous subsidence of the Naturaliste Plateau defined by a new record of volcaniclastic-rich sequence at IODP Site U1513. *Gondwana Research*, *82*, 1–11. https://doi.org/10.1016/j.gr.2019.12.007

Lawver, L. A., Gahagan, L. M., & Coffin, M. F. (1992). The development of paleoseaways around Antarctica. In J. P. Kennett & D. A. Warkne (Eds.), *The Antarctic paleoenvironment: Perspectives on global change: Part one* (pp. 7–30). Washington, DC: American Geophysical Union.

Liu, Z., Zhou, Q., Lai, Y., Qing, C., Li, Y., Wu, J., & Xia, X. (2015). Petrogenesis of the Early Cretaceous Laguila bimodal intrusive rocks from the Tethyan Himalaya: Implications for the break-up of Eastern Gondwana. *Lithos*, *236–237*, 190–202. https://doi.org/10.1016/j.lithos.2015.09.006

Luyendyk, B. P., & Davies, T. A. (1974). Results of DSDP leg 26 and the geologic history of the southern Indian Ocean. In *Initial Reports of the Deep Sea Drilling Project* (Vol. 26, pp. 909–943). Washington, DC: U.S. Government Printing Office. https://doi.org/10.2973/dsdp.proc.26.136.1974

Mahoney, J. J., Jones, W. B., Frey, F. A., Salters, V. J. M., Pyle, D. G., & Davies, H. L. (1995). Geochemical characteristics of lavas from Broken Ridge, the Naturaliste Plateau and southernmost Kerguelen Plateau: Cretaceous plateau volcanism in the southeast Indian Ocean. *Chemical Geology*, *120*, 315–345. https://doi.org/10.1016/0009-2541(94)00144-W

Malinverno, A., Hildebrandt, J., Tominaga, M., & Channell, J. E. T. (2012). M-sequence geomagnetic polarity time scale (MHTC12) that steadies global spreading rates and incorporates astrochronology constraints. *Journal of Geophysical Research*, *117*, B06104. https://doi.org/10.1029/2012JB009260

Maloney, D., Sargent, C., Direen, N. G., Hobbs, R. W., & Grocke, D. R. (2011). Re-evaluation of the Mentelle Basin, a polyphase rifted margin basin, offshore southwest Australia: New insights from integrated regional seismic datasets. *Solid Earth*, *2*, 107–123. https://doi.org/10.5194/se-2-107-2011

Manville, V., Nemeth, K., & Kano, K. (2009). Source to sink: A review of three decades of progress in the understanding of volcaniclastic processes, deposits, and hazards. *Sedimentary Geology*, *220*, 136–161. https://doi.org/10.1016/j.sedgeo.2009.04.022

Maritati, A., Danisik, M., Halpin, J. A., Whittaker, J. M., & Aitken, A. R. A. (2020). Pangea rifting shaped the East Antarctic Landscape. *Tectonics*, *39*, e2020TC006180. https://doi.org/10.1029/2020TC006180

Markl, R. G. (1974). Evidence for the breakup of eastern Gondwanaland by the Early Cretaceous. *Nature*, *251*, 196–200. https://doi.org/10.1038/251196a0

Markl, R. G. (1978). Evidence for the early Cretaceous breakup of Gondwanaland off southwestern Australia. *Marine Geology*, *26*, 41–48. https://doi.org/10.1016/0025-3227(78)90044-0

Martinez, M., Deconinck, J. F., Pellenard, P., Reboulet, S., & Riquier, L. (2013). Astrochronology of the Valanginian Stage from reference sections (Vocontian Basin, France) and palaeoenvironmental implications for the Weissert Event. *Palaeogeography, Palaeoclimatology, Palaeoecology*, *376*, 91–102. https://doi.org/10.1016/j.palaeo.2013.02.021

Mathews, K. J., Seton, M., & Muller, R. D. (2012). A global-scale plate reorganization event at 105−100 Ma. *Earth and Planetary Science Letters*, *355–356*, 283–298. https://doi.org/10.1016/j.epsl.2012.08.023

McKenzie, D. (1978). Some remarks on the development of sedimentary basins. *Earth and Planetary Science Letters*, *40*, 25–32. https://doi.org/10.1016/0012-821X(78)90071-7

McKenzie, D., & Bickle, M. J. (1988). The volume and composition of melt generated by extension of the lithosphere. *Journal of Petrology*, *29*, 625–679. https://doi.org/10.1093/petrology/29.3.625

McKenzie, D., Jackson, J. A., & Priestley, K. (2005). Thermal structure of oceanic and continental lithosphere. *Earth and Planetary Science Letters*, *233*, 337–349. https://doi.org/10.1016/j.epsl.2005.02.005

McPhie, J., Doyle, M., & Allen, R. (1993). *Volcanic textures: A guide to the interpretation of textures in volcanic rocks* (p. 196). Hobart, Australia: Centre for Ore Deposit and Exploration Studies University of Tasmania.

Molnar, P. (2004). Late Cenozoic Increase in Accumulation rates of terrestrial sediment: How might climate change have affected erosion rates? *Annual Review of Earth and Planetary Sciences*, *32*, 67–89. https://doi.org/10.1146/annurev.earth.32.091003.143456

Mulder, T. (2011). Gravity processes and deposits on continental slope, rise and abyssal plains. *Developments in Sedimentology*, *63*, 25–148. https://doi.org/10.1016/B978-0-444-53000-4.00002-0

Müller, R. D., Gaina, C., Tikku, A., Mihut, D., Cande, S. C., & Stock, J. M. (2000). Mesozoic/Cenozoic tectonic events around Australia. In M. A. Richards, R. G. Gordon, & R. D. Van Der Hilst (Eds.), *History and dynamics of global plate motions, geophysical monograph* (Vol. 121, pp. 161–188). Washington, DC: American Geophysical Union.

Mutter, J. C., Hegarty, K. A., Cande, S. C., & Weissel, J. K. (1985). Breakup between Australia and Antarctica: A brief review in the light of new data. *Tectonophysics*, *114*, 255–279. https://doi.org/10.1016/0040-1951(85)90016-2

Mutter, J. C., Talwani, M., & Stoffa, P. (1982). Origin of seaward-dipping reflectors in oceanic crust off the Norwegian margin by subaerial seafloor spreading. *Geology*, *10*, 353–357. https://doi.org/10.1130/0091-7613(1982)10<353:OOSRIO>2.0.CO;2

Norton, I. O., & Sclater, J. G. (1979). A model for the evolution of the Indian Ocean and the breakup of Gondwanaland. *Journal of Geophysical Research*, *84*, 6803–6830. https://doi.org/10.1029/JB084iB12p06803

Norvick, M. S. (2004). *Tectonic and stratigraphic history of the Perth Basin, Geoscience Australia Record 2004/16* (p. 30). Canberra, Australia: Geoscience Australia.

Ogg, J. G., Gabi, M., & Gradstein, F. M. (2016). *A concise geologic time scale* (p. 240). Amsterdam, The Netherlands: Elsevier.

Olierook, H. K. H., Jiang, Q., Jourdan, F., & Chiaradia, M. (2019). Greater Kerguelen large igneous province reveals no role for Kerguelen mantle plume in the continental breakup of eastern Gondwana. *Earth and Planetary Science Letters*, *511*, 244–255. https://doi.org/10.1016/j.epsl.2019.01.037

Olierook, H. K. H., Jourdan, F., & Merle, F. (2019). Age of the Barremian-Aptian boundary and onset of the Cretaceous Normal Superchron. *Earth-Science Reviews*, *197*, 102906. https://doi.org/10.1016/j.earscirev.2019.102906

Olierook, H. K. H., Jourdan, F., Merle, R. E., Timms, N. E., Kusznir, N., & Muhling, J. R. (2016). Bunbury Basalt: Gondwana breakup products or earliest vestiges of the Kerguelen mantle plume? *Earth and Planetary Science Letters*, *440*, 20–32. https://doi.org/10.1016/j.epsl.2016.02.008

Olierook, H. K. H., Merle, R. E., & Jourdan, F. (2017). Toward a Greater Kerguelen large igneous province: Evolving mantle source contributions in and around the Indian Ocean. *Lithos*, *282–283*, 163–172. https://doi.org/10.1016/j.lithos.2017.03.007

Olierook, H. K. H., Merle, R. E., Jourdan, F., Sircombe, K., Faser, G., Timms, N. E., et al. (2015). Age and geochemistry of magmatism on the oceanic Wallaby Plateau and implications for the opening of the Indian Ocean. *Geology*, *43*, 971–974. https://doi.org/10.1130/G37044.1

Owens, R. J., Borissova, I., Hall, L. S., Bernardel, G., Southby, C., Grosjean, E., & Mitchell, C. (2018). *Extensional during rifting direction Geology and prospectivity of the northern Houtman Sub basin, Geoscience Australia Record 2018/25*. Canberra, Australia: Geoscience Australia.

Plumb, K. A. (1979). The tectonic evolution of Australia. *Earth Science Reviews*, *14*, 205–249. https://doi.org/10.1016/0012-8252(79)90001-1

Powell, C. M., Roots, S. R., & Veevers, J. J. (1988). Pre-breakup continental extension in East Gondwanaland and the early opening of the eastern Indian Ocean. *Tectonophysics*, *155*, 261–283. https://doi.org/10.1016/0040-1951(88)90269-7

Presnall, D. C., Gudfinnsson, G. H., & Walter, M. J. (2002). Generation of mid-ocean ridge basalts at pressures from 1 to 7 GPa. *Geochemica et Cosmochimica Acta*, *66*, 2073–2090. https://doi.org/10.1016/S0016-7037(02)00890-6

Putirka, K. (2005). Mantle potential temperatures at Hawaii, Iceland, and the mid-ocean ridge system, as inferred from olivine phenocrysts: Evidence for thermally driven mantle plumes. *Geochemistry, Geophysics, Geosystems*, *6*, Q05L08. https://doi.org/10.1029/2005GC000915

Reading, A. M., Kennett, B. L. N., & Dentith, M. C. (2003). Seismic structure of the Yilgarn Craton, Western Australia. *Australian Journal of Earth Sciences*, *50*(3), 427–438. https://doi.org/10.1046/j.1440-0952.2003.01000.x

Robb, M. S., Taylor, B., & Goodliffe, A. M. (2005). Re-examination of the magnetic lineations of the Gascoyne and Cuvier Abyssal Plains, off NW Australia. *Geophysical Journal International*, *163*, 42–55. https://doi.org/10.1111/j.1365-246X.2005.02727.x

Royer, J.-Y., & Sandwell, D. T. (1989). Evolution of the eastern Indian ocean since the Late Cretaceous: Constraints from GEOSAT altimetry. *Journal of Geophysical Research*, *94*, 13755–13782. https://doi.org/10.1029/JB094iB10p13755

Sayers, J., Symonds, P. A., Direen, N. G., Bernadel, G. (2001), Nature of the continent–ocean transition on the non-volcanic rifted margin of the central Great Australian Bight. In R. C. L. Wilson, R. B. Whitmarsh, B. Taylor, & N. Froitzheim (Eds.), *Non-volcanic Rifting of continental margins: A comparison of evidence from land and sea* (Vol. 187, pp. 51–76). London: Geological Society. https://doi.org/10.1144/GSL.SP.2001.187.01.04

Saygin, E., & Kennett, B. L. N. (2012). Crustal structure of Australia from ambient seismic noise tomography. *Journal of Geophysical Research*, *117*, B01304. https://doi.org/10.1029/2011JB008403

Sircombe, K. N., & Freeman, M. J. (1999). Provenance of detrital zircons on the Western Australia coastline—Implications for the geologic history of the Perth basin and denudation of the Yilgarn craton. *Geology*, *27*, 879–882. https://doi.org/10.1130/0091-7613(1999)027<0879:PODZOT>2.3.CO;2

Song, T., & Cawood, P. S. (2000). Structural styles in the Perth Basin associated with the Mesozoic break-up of Greater India and Australia. *Tectonophysics*, *317*, 55–72. https://doi.org/10.1016/S0040-1951(99)00273-5

Steckler, M. S., & Watts, A. B. (1978). Subsidence of the Atlantic-type continental margin off New York. *Earth and Planetary Science Letters*, *41*, 1–13. https://doi.org/10.1016/0012-821X(78)90036-5

Storey, M., Saunders, A. D., Tarney, J., Gibson, I. L., Norry, M. J., Thirlwall, M. F., et al. (1989). Contamination of Indian Ocean astheno-sphere by the Kerguelen-Heard mantle plume. *Nature*, *338*, 574–576. https://doi.org/10.1038/338574a0

Storey, M., Kent, R. W., Saunders, A. D., Salters, V. J., Hergt, J., Whitechurch, H., et al. (1992). Lower Cretaceous volcanic rocks on continen-tal margins and their relationship to the Kerguelen Plateau. S. W. Wise & R. Schlich *Proceedings of the Ocean Drilling Program, Scientific Results*, 120, (33–53). College Station, TX: Ocean Drilling Program. https://doi.org/10.2973/odp.proc.sr.120.118.1992

Symonds, P. A., Planke, S., Frey, O., & Skogseid, J. (1998). Volcanic evolution of the Western Australian continental margin and its impli-cations for basin development. In P. G. Purcell, & R. R. Purcell (Eds.), *The sedimentary basins of Western Australia 2* (pp. 33–54). Perth, Australia: Petroleum Exploration Society of Australia.

Tejada, M. L. G., Lee, E. Y., Chun, S. S., Harry, D. L., Riquier, L. Wainman, C. C. (2020), *Data report: Petrology and volcanic stratigraphy at Site U1513, IODP Expedition 369* (Vol. 369, Australia Cretaceous climate and tectonics). Proceedings of the International Ocean Discov-ery Program, International Ocean Discovery Program, College Station, TX. https://doi.org/10.14379/iodp.proc.369.202.2020

Tikku, A. A., & Cande, S. C. (1999). The oldest magnetic anomalies in the Australian-Antarctic Basin: Are they isochrons? *Journal of Geophysical Research*, *104*, 661–677. https://doi.org/10.1029/1998JB900034

Tikku, A. A., & Direen, N. G. (2008). Comment on "major Australian-Antarctic plate reorganization at Hawaiian-Emperor bend time". *Science*, *321*, 490. https://doi.org/10.1126/science.1157163

Veevers, J. J. (1986). Breakup of Australia and Antarctica estimated as Mid-Cretaceous (95+5 Ma) from magnetic and seismic data at the continental margin. *Earth and Planetary Science Letters*, *77*, 91–99. https://doi.org/10.1016/0012-821X(86)90135-4

Veevers, J. J. (2006). Updated Gondwana (Permian-Cretaceous) earth history of Australia. *Gondwana Research*, *9*, 231–260. https://doi.org/10.1016/j.gr.2005.11.005

Wainman, C. C., Borissova, I., Harry, D. L., Hobbs, R. W., Mantle, D. J., Maritati, A., et al. (2020), Evidence for non-marine Jurassic to ear-liest Cretaceous sediments in the pre-breakup section of the Mentelle Basin. *Australian Journal of Earth Sciences*, *67*, 89–105. https://doi.org/10.1080/08120099.2019.1627581

Wallace, P. J. (2002). Volatiles in submarine basaltic glasses from the Northern Kerguelen Plateau (ODP Site 1140): Implications for source region compositions, shallow magmatic processes and plateau subsidence. *Journal of Petrology*, *43*, 1311–1326. https://doi.org/10.1093/petrology/43.7.1311

Wallace, P. J., Frey, F. A., Weis, D., & Coffin, M. F. (2002). Origin and evolution of the Kerguelen Plateau, Broken Ridge and Kerguelen archipelago: Editorial. *Journal of Petrology*, *43*(7), 1105–1108. https://doi.org/10.1093/petrology/43.7.1105

Watson, S. J., Whittaker, J. M., Halpin, J. A., Williams, S. E., Milan, L. A., Daczko, N. R., & Wyman, D. A. (2016). Tectonic drivers and the influence of the Kerguelen plume on seafloor spreading during formation of the early Indian Ocean. *Gondwana Research*, *35*, 97–114. https://doi.org/10.1016/j.gr.2016.03.009

Weis, D., & Frey, F. A. (2002). Submarine basalts of the Northern Kerguelen Plateau: Interaction between the Kerguelen Plume and the Southeast Indian Ridge revealed at ODP Site 1140. *Journal of Petrology*, *43*, 1287–1310. https://doi.org/10.1093/petrology/43.7.1287

Whitechurch, H., Montigny, R., Sevigny, J., Storey, M., & Salters, V. (1992). K-Ar and 40Ar-39Ar ages of central Kerguelen Plateau basalts (Vol. 120, pp. 71–77). Proceedings of the Ocean Drilling Program, Scientific Results, Ocean Drilling Program, College Station, TX.

White, L. T., Gibson, G. M., & Lister, G. S. (2013). A reassessment of paleogeographic reconstructions of eastern Gondwana: Bringing geology back into the equation. *Gondwana Research*, *24*, 984–998. https://doi.org/10.1016/j.gr.2013.06.009

White, R. S., & McKenzie, D. (1995). Mantle plumes and flood basalts. *Journal of Geophysical Research*, *100*, 17543–17585. https://doi.org/10.1029/95JB01585

Whittaker, J. M., Halpin, J. A., Williams, S. E., Hall, L. S., Gardner, R., Kobler, M. E., et al. (2013). Tectonic evolution and continental frag-mentation of the southern West Australian margin. In S. J. Moss, & M. Keep (Eds.), *West Australian Basins Symposium* (pp. 1–16). Perth, Australia: Petroleum Exploration Society of Australia.

Whittaker, J. M., Williams, S. E., Halpin, J. A., Wild, T. J., Stilwell, J. D., Jourdan, F., & Daczko, R. (2016). Eastern Indian Ocean mi-crocontinent formation driven by plate motion changes. *Earth and Planetary Science Letters*, *454*, 203–212. https://doi.org/10.1016/j.epsl.2016.09.019

Williams, S. E., Whittaker, J. M., Granot, R., & Müller, R. D. (2013). Early India-Australia spreading history revealed by newly detected Mesozoic magnetic anomalies in the Perth Abyssal Plain. *Journal of Geophysical Research: Solid Earth*, *118*, 3275–3284. https://doi.org/10.1002/jgrb.50239

Williams, S. E., Whittaker, J. M., & Müller, R. D. (2011). Full-fit, palinspastic reconstruction of the conjugate Australian-Antarctic margins. *Tectonics*, *30*, TC6012. https://doi.org/10.1029/2011TC002912

Yeates, A. N., Bradshaw, M. T., Dickins, J. M., Brakel, A. T., Exon, N. F., Langford, R. P., et al. (1987). The Westralian superbasin: An Aus-tralian link with Tethys. In K. G. McKenzie (Ed.), *International Symposium on Shallow Tethys 2* (pp. 199–213). Wagga Wagga, Rotterdam, The Netherlands: A. A. Balkema.

Zhou, Q., Liu, Z., Lai, Y., Wang, G.-C., Liao, Z., Li, Y.-X., et al. (2017). Petrogenesis of mafic and felsic rocks from the Comei large igneous province, South Tibet: Implications for the initial activity of the Kerguelen plume. *Geological Society of America Bulletin*, *130*, 811–824. https://doi.org/10.1130/B31653.1

Zhu, D.-C., Chung, S.-L., Mo, X.-X., Zhao, Z.-D., Niu, Y., Song, B., & Yang, Y.-H. (2009). The 132 Ma Comei-Bunbury large igneous prov-ince: Remnants identified in present-day southeastern Tibet and southwestern Australia. *Geology*, *37*, 583–586. https://doi.org/10.1130/G30001A.1

Zhu, D. -C., Mo, X., Pan, G., Zhao, Z., Dong, G., Shi, Y., et al. (2008). Petrogenesis of the earliest Early Cretaceous mafic rocks from the Cona area of the eastern Tethyan Himalaya in south Tibet: Interaction between the incubating Kerguelen plume and the eastern Greater India lithosphere? *Lithos*, *100*, 147–175. https://doi.org/10.1016/j.lithos.2007.06.024